9 Applications of Models of Offshore Structures

Each offshore structure is unique in the sense that it is built only after a customer with a specific need actually places an order. Design companies and manufacturers of engineering systems of this type are often small and medium enterprises, which cannot afford purchasing costly computer software packages for numerical computation involved in dynamics of mechanical systems. Therefore, they often employ custom, in-house dynamic models of the structures designed. In the present chapter, dynamic models of the following are presented: a gantry suited for relocating sets of BOP valves on an extraction platform, a column crane and a device for laying pipes on the seabed. The formulation of models thereof leverages the methods described in earlier chapters.

9.1 BOP Transportation Gantry

One of the types of offshore cranes is a BOP crane. The construction of Protea from Gdańsk is presented in Fig. 9.1. It is a gantry crane installed on a drilling platform designed to transport a system of valves named BOP (Blowout Preventor). BOP is used to block an uncontrolled outflow of oil or natural gas from a wellbore at the seabed. After drilling the wellbore, the BOP is put inside it, and afterwards risers are being connected to the BOP. The risers drain off oil or gas into suitable tanks. In view of the plug task, weight of the BOP reaches hundreds of tons. During the transportation process (during the travel of a gantry crane) the BOP is protected by a system of guides presented in Fig. 9.2.

Clearance between the load and the guide system equals a few centimetres. Weight of the presented crane is 200 T, hoisting capacity 550 T and height about 30 m. The analysis of a travel system is an interesting and important problem concerning the dynamics of a BOP crane. The crane is supported on rails and its motion is realized by the means of a rack and a toothed wheel (Fig. 9.3). Maximum velocity of travel of the crane is equal to 3 m/min. Due to the movement of the platform's deck caused by sea weaving and wind forces, the protection systems are used. These systems limit the movement of the crane in vertical direction and horizontal one, perpendicular to the longitudinal axis of rails. This task is particularly realized by an anti-lift system presented in Fig. 9.4.

E. Wittbrodt et al.: Rigid Finite Element Method, OEO 1, pp. 139–201.
springerlink.com

Fig. 9.1. BOP crane

Fig. 9.2. Guide system

Fig. 9.3. Rack travel system

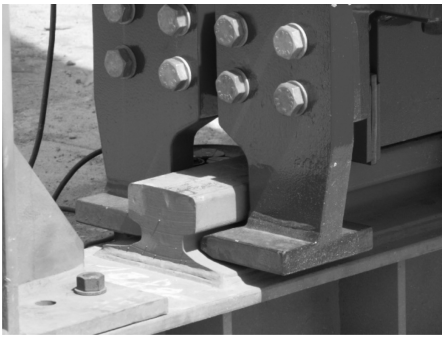

Fig. 9.4. Anti-lift system

9.1.1 Mathematical Model of the System

The schema of the model of the BOP crane together with more important coordinate systems is presented in Fig. 9.5. The following basic assumptions for modelling are established:

- movement of the base (system $\{A\}$) is known and described by functions:

$$\begin{aligned} y_1 &= x_{org}^{(A)}(t); \quad y_2 = x_{org}^{(A)}(t); \quad y_3 = x_{org}^{(A)}(t); \\ y_6 &= \psi_{org}^{(A)}(t); \quad y_5 = \theta_{org}^{(A)}(t); \quad y_4 = \varphi_{org}^{(A)}(t), \end{aligned} \tag{9.1}$$

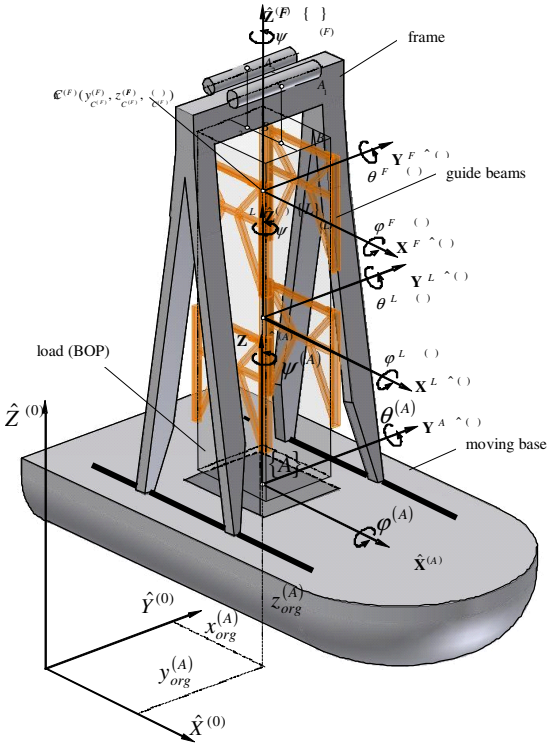

Fig. 9.5. A model of a BOP gantry with load

- structure of the crane (frame) is treated as a rigid body – it should be noticed that the construction of the BOP crane is a kind of combination of two A-frames; an A-frame has been a subject of many analyses presented in [Fałat P., 2004]; these analyses have shown that the influence of flexibility of the frame on dynamics of the whole system (on motion of the load) is slight,
- load is a rigid body of rectangular shape,
- load is suspended on two ropes – their flexibility and damping are taken into account,
- load can touch the guides only along its edges,
- clearance and flexibility between the load and guides are taken into consideration,
- frame is fixed flexibly to the deck and, additionally, in $\hat{\mathbf{Y}}^{(A)}$ direction clearance can occur,
- input in the drive system has been modelled in two ways: a kinematic input via a spring-damping element and a force input,
- wind force can be taken into consideration,
- homogenous transformations are used to describe the system's geometry.

Both the load (system $\{L\}$ in Fig. 9.5) and the frame (system $\{F\}$) have 6 degrees of freedom in respect to the deck (system $\{A\}$). So, the model has 12 degrees of freedom and the vector of generalized coordinates of the system has a following form:

$$\mathbf{q} = \begin{bmatrix} \mathbf{q}^{(F)} \\ \mathbf{q}^{(L)} \end{bmatrix}, \tag{9.2}$$

where $\mathbf{q}^{(F)} = \begin{bmatrix} x^{(F)} & y^{(F)} & z^{(F)} & \psi^{(F)} & \theta^{(F)} & \varphi^{(F)} \end{bmatrix}^T$,

$\mathbf{q}^{(L)} = \begin{bmatrix} x^{(L)} & y^{(L)} & z^{(L)} & \psi^{(L)} & \theta^{(L)} & \varphi^{(L)} \end{bmatrix}^T$.

It has been mentioned that the motion of the base (deck of the platform), that means the motion of the system $\{A\}$, in respect to the inertial coordinate system $\{\}$ has been assumed as known, described by pseudo-harmonic functions:

$$y_i = \sum_{j=1}^{n_i^{(A)}} A_{i,j}^{(A)} \sin\left(\omega_{i,j}^{(A)} t + \varphi_{i,j}^{(A)}\right) \qquad i = 1,\ldots,6, \tag{9.3}$$

where $A_{i,j}^{(A)}, \omega_{i,j}^{(A)}, \varphi_{i,j}^{(A)}$ – amplitude, angular frequency and phase angle of the input, respectively,

$n_i^{(A)}$ – number of harmonics of the series.

The application of homogenous transformations allows converting a position vector of the point defined in the system $\{A\}$ to system $\{\}$ according to relation:

$$\mathbf{r}_p^{\{\}} = {}_A^0\mathbf{T}\,\mathbf{r}_P^{\{A\}}, \tag{9.4}$$

where $\mathbf{r}_p^{\{\}} = \begin{bmatrix} x_p & y_p & z_p & 1 \end{bmatrix}^T$ – position vector of point P in the inertial system $\{\}$,

$\mathbf{r}_P^{\{A\}} = \begin{bmatrix} x_P^{\{A\}} & y_P^{\{A\}} & z_P^{\{A\}} & 1 \end{bmatrix}^T$ – position vector of point P in the system $\{A\}$,

${}_A^0\mathbf{T}$ – matrix of a homogenous transformation from the system {A} to the system $\{\}$.

The matrix ${}_A^0\mathbf{T}$ can be presented as product of six matrices, where each of them is a function of one variable dependent on time (9.4). Order of rotations included in the matrix ${}_A^0\mathbf{T}$ corresponds to Euler angles ZYX.

Kinetic and Potential Energy of the Frame and the Load

Kinetic and potential energy of the frame, as well as the load, can be determined using general algorithms presented in chapter 5. If one denotes the homogenous

transformation matrix from the frame system $\{F\}$ to the deck system $\{A\}$ as $\tilde{\mathbf{T}}^{(F)}$ and from the load system $\{L\}$ as $\tilde{\mathbf{T}}^{(L)}$, the transformation matrices from the frame system and from the load system to the system $\{\}$ can be calculated as:

$$\mathbf{T}^{(F)} = {}^{0}_{A}\mathbf{T}\,\tilde{\mathbf{T}}^{(F)}, \tag{9.5}$$

$$\mathbf{T}^{(L)} = {}^{0}_{A}\mathbf{T}\,\tilde{\mathbf{T}}^{(L)}. \tag{9.6}$$

Introducing notation of the Lagrange operator:

$$\varepsilon_k^{(b)} = \frac{d}{dt}\frac{\partial E^{(b)}}{\partial \dot{q}_k^{(b)}} - \frac{\partial E^{(b)}}{\partial q_k^{(b)}}, \tag{9.7}$$

where k is the number of the generalized coordinate, $b \in \{F, L\}$,
and using the transformation presented in chapter 5 one can obtain:

$$\varepsilon_k^{(b)} = tr\left\{ \mathbf{T}_k^{(b)}\mathbf{H}^{(b)}\left[{}^{0}_{A}\ddot{\mathbf{T}}\tilde{\mathbf{T}}^{(b)} + 2{}^{0}_{A}\dot{\mathbf{T}}\dot{\tilde{\mathbf{T}}}^{(b)} + \sum_{i=1}^{6}\sum_{j=1}^{6}\mathbf{T}_{i,j}^{(b)}\dot{q}_i^{(b)}\dot{q}_j^{(b)} + \sum_{i=1}^{6}\mathbf{T}_i^{(b)}\ddot{q}_i^{(b)} \right] \right\}, \tag{9.8}$$

where $\mathbf{T}_k^{(b)} = \dfrac{\partial \mathbf{T}^{(b)}}{\partial q_k^{(b)}}$,

$$\mathbf{T}_{i,j}^{(b)} = \frac{\partial^2 \mathbf{T}^{(b)}}{\partial q_i^{(b)} \partial q_j^{(b)}}.$$

The above form requires repeated multiplication of matrices of 4×4 dimensions and then the calculation of the trace of the result matrices. In order to decrease the number of required numerical operations, the authors decided to derive formulae describing Lagrange operators in the explicit form.

The relation (9.8) can be presented in the following form:

$$\begin{aligned}
\varepsilon_k^{(b)} &= \mathrm{tr}\left\{ {}^{0}_{A}\mathbf{T}\tilde{\mathbf{T}}_k^{(b)}\mathbf{H}^{(b)}\left[{}^{0}_{A}\ddot{\mathbf{T}}\tilde{\mathbf{T}}^{(b)} + 2{}^{0}_{A}\dot{\mathbf{T}}\dot{\tilde{\mathbf{T}}}^{(b)} + {}^{0}_{A}\mathbf{T}\ddot{\tilde{\mathbf{T}}}^{(b)} \right]^T \right\} = \\
&= \underbrace{\mathrm{tr}\left\{ {}^{0}_{A}\mathbf{T}^T\,{}^{0}_{A}\mathbf{T}\tilde{\mathbf{T}}_k^{(b)}\mathbf{H}^{(b)}\left[\ddot{\tilde{\mathbf{T}}}^{(b)} \right]^T \right\}}_{\varepsilon_{k,2}^{(b)}} + \underbrace{\mathrm{tr}\left\{ \left[{}^{0}_{A}\ddot{\mathbf{T}}^T\,{}^{0}_{A}\mathbf{T}\tilde{\mathbf{T}}_k^{(b)}\mathbf{H}^{(b)}\left[\tilde{\mathbf{T}}^{(b)} \right]^T \right\}}_{\varepsilon_{k,0}^{(b)}} \\
&+ \underbrace{2\mathrm{tr}\left\{ {}^{0}_{A}\dot{\mathbf{T}}^T\,{}^{0}_{A}\mathbf{T}\tilde{\mathbf{T}}_k^{(b)}\mathbf{H}^{(b)}\left[\dot{\tilde{\mathbf{T}}}^{(b)} \right]^T \right\}}_{\varepsilon_{k,1}^{(b)}}.
\end{aligned} \tag{9.9}$$

Assuming that rotation angles of the frame and the load are small, the matrix $\tilde{\mathbf{T}}^{(b)}$ can be written as:

$$\tilde{\mathbf{T}}^{(b)} = \begin{bmatrix} 1 & -\psi^{(b)} & \theta^{(b)} & x^{(b)} \\ \psi^{(b)} & 1 & -\varphi^{(b)} & y^{(b)} \\ -\theta^{(b)} & \varphi^{(b)} & 1 & z^{(b)} \\ 0 & 0 & 0 & 1 \end{bmatrix} \tag{9.10}$$

or:

$$\tilde{\mathbf{T}}^{(b)} = \mathbf{I} + \sum_{j=1}^{6} \mathbf{D}_j q_j^{(b)}, \tag{9.11}$$

where $q_j^{(b)}$ – suitable elements of vectors $\mathbf{q}^{(F)}$ or $\mathbf{q}^{(L)}$,

and matrices $\mathbf{D}_j$ can be defined as:

for *j*=1,2,3:

$$\mathbf{D}_j = \begin{bmatrix} \mathbf{0} & \mathbf{a}_j \\ \mathbf{0} & 0 \end{bmatrix}, \tag{9.12}$$

where $\mathbf{a}_1 = \begin{bmatrix} 1 \\ 0 \\ 0 \end{bmatrix}$; $\mathbf{a}_2 = \begin{bmatrix} 0 \\ 1 \\ 0 \end{bmatrix}$; $\mathbf{a}_3 = \begin{bmatrix} 0 \\ 1 \\ 0 \end{bmatrix}$,

for *j*=4,5,6:

$$\mathbf{D}_j = \begin{bmatrix} \mathbf{R}_j & \mathbf{0} \\ \mathbf{0} & 0 \end{bmatrix}, \tag{9.13}$$

where $\mathbf{R}_4 = \begin{bmatrix} 0 & 0 & 0 \\ 0 & 0 & -1 \\ 0 & 1 & 0 \end{bmatrix}$, $\mathbf{R}_5 = \begin{bmatrix} 0 & 0 & 1 \\ 0 & 0 & 0 \\ -1 & 0 & 0 \end{bmatrix}$, $\mathbf{R}_6 = \begin{bmatrix} 0 & -1 & 0 \\ 1 & 0 & 0 \\ 0 & 0 & 0 \end{bmatrix}$.

In the paper [Urabś A., et al., 2010] it has been shown that:

for k=1,2,3:

$$\varepsilon_{k,2}^{(b)} = m^{(b)} \ddot{q}_k^{(b)}, \tag{9.14}$$

$$\varepsilon_{k,1}^{(b)} = \sum_{j=1}^{3} \dot{q}_j^{(b)} m^{(b)} \left(\mathbf{\Phi}_1^T \mathbf{\Phi}_0 \right)_{j,k}, \tag{9.15}$$

$$\varepsilon_{k,0}^{(b)} = m^{(b)}, \tag{9.16}$$

for k=4,5,6:

$$\varepsilon_{k,1}^{(b)} = \sum_{j=4}^{6} \dot{q}_j^{(b)} \operatorname{tr}\left(\mathbf{\Phi}_1^T \mathbf{\Phi}_0 \mathbf{R}_k^{(b)} \mathbf{J}^{(b)} \left[\mathbf{R}_j^{(b)} \right]^T \right)_{j,k}, \tag{9.17}$$

$$\varepsilon_{4,2}^{(b)} = \left(J_{11}^{(b)} + J_{22}^{(b)} \right) \ddot{q}_4^{(b)} - J_{32}^{(b)} \ddot{q}_5^{(b)} - J_{31}^{(b)} \ddot{q}_6^{(b)}, \tag{9.18.1}$$

$$\varepsilon_{5,2}^{(b)} = -J_{23}^{(b)} \ddot{q}_4^{(b)} + \left(J_{11}^{(b)} + J_{33}^{(b)} \right) \ddot{q}_5^{(b)} - J_{21}^{(b)} \ddot{q}_6^{(b)}, \tag{9.18.2}$$

$$\varepsilon_{6,2}^{(b)} = -J_{13}^{(b)} \ddot{q}_4^{(b)} - J_{12}^{(b)} \ddot{q}_5^{(b)} + \left(J_{22}^{(b)} + J_{33}^{(b)} \right) \ddot{q}_6^{(b)}, \tag{9.18.3}$$

$$\varepsilon_{k,0}^{(b)} = \operatorname{tr}\left\{ \mathbf{\Phi}_2^T \mathbf{\Phi}_0 \mathbf{R}_k^{(b)} \mathbf{J}^{(b)} \right\} + \sum_{j=4}^{6} q_j^{(b)} \operatorname{tr}\left\{ \mathbf{\Phi}_2^T \mathbf{\Phi}_0 \mathbf{R}_k^{(b)} \mathbf{J}^{(b)} \left[\mathbf{R}_j^{(b)} \right]^T \right\}, \tag{9.19}$$

where $m^{(b)}$ – mass of the body $b \in \{F, L\}$,

$\mathbf{J}^{(b)} = \begin{bmatrix} J_{11}^{(b)} & J_{12}^{(b)} & J_{13}^{(b)} \\ J_{21}^{(b)} & J_{22}^{(b)} & J_{23}^{(b)} \\ J_{31}^{(b)} & J_{32}^{(b)} & J_{33}^{(b)} \end{bmatrix}$ – elements of the matrix are defined in (5.11),

$\mathbf{\Phi}_0, \mathbf{\Phi}_1, \mathbf{\Phi}_2, \mathbf{S}_0, \mathbf{S}_1, \mathbf{S}_2$ – submatrices of ${}_A^0\mathbf{T}$, ${}_A^0\dot{\mathbf{T}}$, ${}_A^0\ddot{\mathbf{T}}$ respectively,

${}_A^0\mathbf{T} = \begin{bmatrix} \mathbf{\Phi}_0 & \mathbf{S}_0 \\ \mathbf{0} & 1 \end{bmatrix}$, ${}_A^0\dot{\mathbf{T}} = \begin{bmatrix} \mathbf{\Phi}_1 & \mathbf{S}_1 \\ \mathbf{0} & 0 \end{bmatrix}$, ${}_A^0\ddot{\mathbf{T}} = \begin{bmatrix} \mathbf{\Phi}_2 & \mathbf{S}_2 \\ \mathbf{0} & 0 \end{bmatrix}$.

Derivatives of potential energy of gravity forces of element of mass $m^{(b)}$ can be presented in the form of the vector:

$$\frac{\partial V_g^{(b)}}{\partial \mathbf{q}^{(b)}} = \begin{bmatrix} m^{(b)} g\, t_{31} & m^{(b)} g\, t_{32} & m^{(b)} g\, t_{33} & 0 & 0 & 0 \end{bmatrix}^T, \tag{9.20}$$

where $\mathbf{q}^{(b)}$ – vector of coordinates of the frame or the load (defined in (9.2)), respectively,

$m^{(b)}$ – mass of the frame or the load,

t_{31}, t_{33}, t_{33} – proper elements of the third row of the matrix ${}_A^0\mathbf{T}$.

Model of the Support

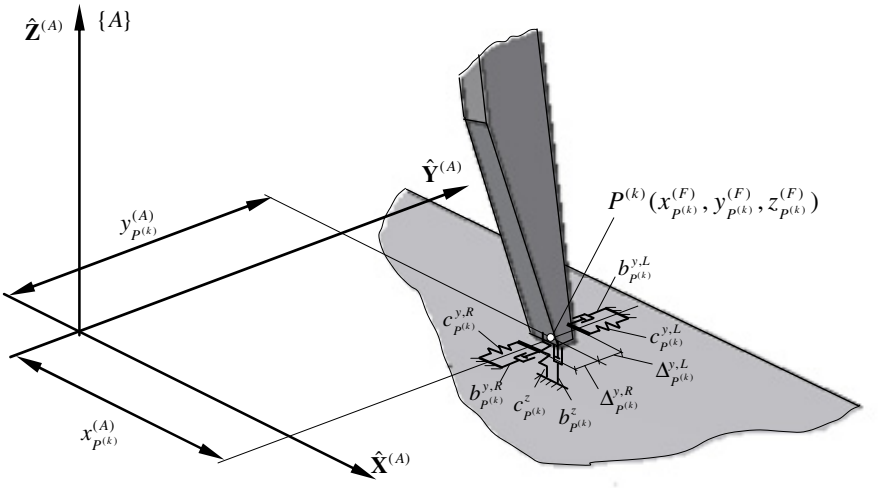

Fig. 9.6. Flexible connection of the frame to the deck

It has been assumed that the frame of the BOP crane is supported flexibly in four points denoted as $P^{(k)}$ $(k = 1,2,3,4)$. The crane is moving on a dedicated rail system in direction parallel to $\hat{\mathbf{X}}^{(A)}$ axis (Fig.9.6). Additionally, a constructional clearance can occur in $\hat{\mathbf{Y}}^{(A)}$ direction.
The reaction force, i. e. the reaction force of the base on the frame, is depicted by the vector:

$$\mathbf{F}^{(F)}_{P^{(k)}} = \left[F^{(F,x)}_{P^{(k)}} \quad F^{(F,y)}_{P^{(k)}} \quad F^{(F,z)}_{P^{(k)}}\right]^T. \tag{9.21}$$

The $F^{(F,z)}_{P^{(k)}}$ component can be calculated as:

$$F^{(F,z)}_{P^{(k)}} = F^{(F,z)}_{S,P^{(k)}} + F^{(F,z)}_{D,P^{(k)}}, \tag{9.22}$$

where $F^{(F,z)}_{S,P^{(k)}}$ – stiffness force,

$F^{(F,z)}_{D,P^{(k)}}$ – damping force.

The stiffness and damping forces are determined by relations:

$$F_{S,P^{(k)}}^{(F,z)} = -c_{P^{(k)}}^{z} \delta_{P^{(k)}}^{z} \Delta z_{P^{(k)}}, \tag{9.23.1}$$

$$F_{D,P^{(k)}}^{(F,z)} = -b_{P^{(k)}}^{z} \delta_{P^{(k)}}^{z} \Delta \dot{z}_{P^{(k)}}, \tag{9.23.2}$$

where $\delta_{P^{(k)}}^{z} = \begin{cases} 1 \text{ when } \Delta z_{P^{(k)}} < 0 \\ 0 \text{ when } \Delta z_{P^{(k)}} \geq 0 \end{cases}$

$\Delta z_{P^{(k)}} = z_{P^{(k)}}^{(A)} - z_{P^{(k)}}^{(A,0)}$, where $z_{P^{(k)}}^{(A,0)} = 0$, and $z_{P^{(k)}}^{(A)}$ is the z coordinate of the point $P^{(k)}$ in the system $\{A\}$, $\Delta \dot{z}_{P^{(k)}} = \dot{z}_{P^{(k)}}^{(A)}$,

$c_{P^{(k)}}^{z}, b_{P^{(k)}}^{z}$ – stiffness and damping coefficients of the connection in the $\hat{\mathbf{Z}}^{(A)}$ direction, respectively.

In the case of the component $F_{P^{(k)}}^{(F,y)}$, the possibility of occurrence of clearance in the anti-lift system is taken into account. Due to modelling clearance, two spring-damping elements acting in the $\hat{\mathbf{Y}}^{(A)}$ direction are introduced, as described in chapter 6.2.

The component $F_{P^{(k)}}^{(F,x)}$ from (9.21) can be expressed by:

$$F_{P^{(k)}}^{(F,x)} = -\operatorname{sgn}(\upsilon_{P^{(k)}}^{(A,x)}) S_{P^{(k)}}^{(F,x)}(F_{P^{(k)}}^{(F,y)}, F_{P^{(k)}}^{(F,z)}) \tag{9.24}$$

where $S_{P^{(k)}}^{(F,x)}$ – resisting force caused by rolling or sliding friction,

$\upsilon_{P^{(k)}}^{(A,x)}$ – component x of the velocity of the point $P^{(k)}$ in the coordinate system $\{A\}$.

After calculating suitable coordinates and velocity of points of support, generalized force of flexible connection of the frame and the deck can be written as:

$$\mathbf{Q}_{P^{(k)}}^{(F)} = \mathbf{U}_{P^{(k)}}^{(F)^T} \mathbf{F}_{P^{(k)}}^{(F)}, \tag{9.25}$$

where $\mathbf{U}_{P^{(k)}}^{(F)} = \begin{bmatrix} 1 & 0 & 0 & -y_{P^{(k)}}^{(F)} & z_{P^{(k)}}^{(F)} & 0 \\ 0 & 1 & 0 & x_{P^{(k)}}^{(F)} & 0 & -z_{P^{(k)}}^{(F)} \\ 0 & 0 & 1 & 0 & -x_{P^{(k)}}^{(F)} & y_{P^{(k)}}^{(F)} \end{bmatrix}$.

Generalizing the relation (9.25) to four supports one can obtain:

$$\mathbf{Q}_p^{(F)} = \sum_{k=1}^{4} \mathbf{Q}_{P^{(k)}}^{(F)} = \sum_{k=1}^{4} \mathbf{U}_{P^{(k)}}^{(F)^T} \mathbf{F}_{P^{(k)}}^{(F)} . \tag{9.26}$$

Modelling Clearance between the Load and Guides

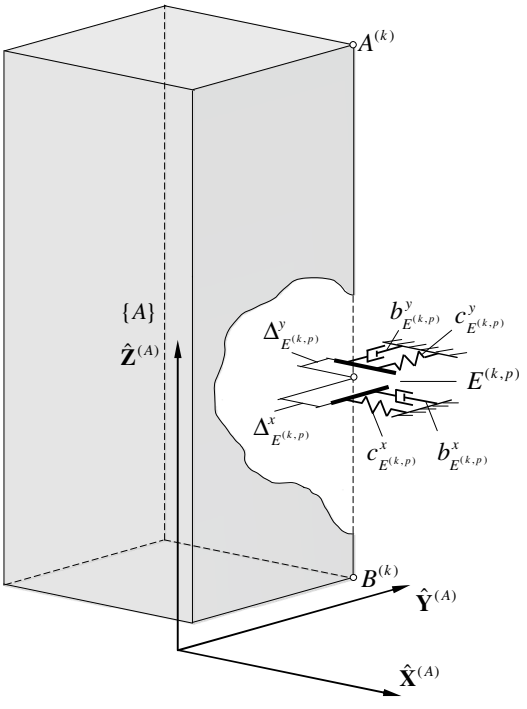

Fig. 9.7. Load and spring-damping elements with clearance

The guides have been replaced by spring-damping elements with clearance (SDE $E^{(kp)}$) that limited the movement of the load in $\hat{\mathbf{X}}^{(A)}$ and $\hat{\mathbf{Y}}^{(A)}$ directions (Fig. 9.7). It has been assumed that the load can contact with guides only along its edges and the number of spring-damping elements can be different for each edge. The manner of calculation of stiffness and damping forces coming from the each side is analogical to the one presented in chapter 5.3. Additionally, one has to determine equivalent coefficients of flexibility of elements modelling the guides. Suitable calculations have been executed by the means of the Finite Elements Method. They were presented in details in the doctoral thesis [Urbaś A., 2011].

Drive of Travel System

The input in the drive of the travel system has been modelled in two ways (Fig. 9.8): a kinematic input via a spring-damping element (flexible) and a force input (rigid). It has been assumed that the drive acts in points $P^{(1)}$ and $P^{(4)}$.

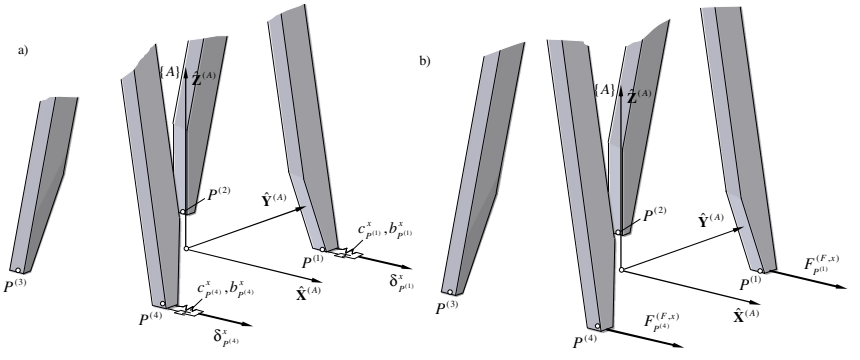

Fig. 9.8. The travel system of the crane: a) flexible, b) rigid

1. Kinematic input

In this case, the potential energy of elastic deformation and the dissipation function of the drive system can be calculated as:

$$V_t^{(i)} = \frac{1}{2} c^x_{P^{(i)}} \left[\delta^x_{P^{(i)}}(t) - x^{(A)}_{P^{(i)}} \right]^2$$
$$D_t^{(i)} = \frac{1}{2} b^x_{P^{(i)}} \left[\dot{\delta}^x_{P^{(i)}}(t) - \dot{x}^{(A)}_{P^{(i)}} \right]^2 \qquad i=1,4 \qquad (9.27)$$

where $\delta^x_{P^{(1)}}(t),\ \delta^x_{P^{(4)}}(t)$ – assumed displacement (kinematic input),

$c^x_{P^{(i)}}, b^x_{P^{(i)}}$ – stiffness and damping coefficients of the drive of the travel system, respectively.

After determining coordinates $x^{(A)}_{P^{(i)}}$ as function of elements of vector $\mathbf{q}^{(F)}$, one should place suitable derivatives in the equations of motion of the system.

2. Force input

In the case of force input, the unknown forces $F^{(F)}_{P^{(1)}}$, $F^{(F)}_{P^{(4)}}$ and suitable constrains equations have been introduced. Generally, the forces can be placed on the left side of the equations of motion of the system which can be written as:

$$\mathbf{A}\ddot{\mathbf{q}} - \mathbf{DF} = \mathbf{f}\,, \tag{9.28}$$

where $\mathbf{D} = \begin{bmatrix} \mathbf{0} & \mathbf{0} \\ \mathbf{U}_{P^{(1)},1}^{(F)T} & \mathbf{U}_{P^{(4)},1}^{(F)T} \end{bmatrix}$,

$\mathbf{F} = \begin{bmatrix} F_{P^{(1)}}^{(F)} \\ F_{P^{(4)}}^{(F)} \end{bmatrix}$,

$\mathbf{U}_{P^{(1)},1}^{(F)T}, \mathbf{U}_{P^{(4)},1}^{(F)T}$ – the first rows of the matrices from (9.25).

In the analysed problem, the constrains equations have the form:

$$x_{P^{(1)}}^{(D)} = \delta_{P^{(1)}}^{x}(t)\,, \tag{9.29.1}$$

$$x_{P^{(4)}}^{(D)} = \delta_{P^{(4)}}^{x}(t)\,. \tag{9.29.2}$$

Due to convenience of the computer implementation, they can be presented in the matrix and acceleration form:

$$\mathbf{D}^T\ddot{\mathbf{q}} = \ddot{\boldsymbol{\delta}} = \begin{bmatrix} \ddot{\delta}_{P^{(1)}}^{x}(t) \\ \ddot{\delta}_{P^{(4)}}^{x}(t) \end{bmatrix}. \tag{9.30}$$

Energy of Elastic Deformation and Energy Dissipation of the Ropes

The load is suspended on two ropes, so their energy of elastic deformation can be written as:

$$V_r^{(p)} = \sum_{p=1}^{2} \frac{1}{2} c_r^{(p)} \delta_r^{(p)} \left[\Delta l_{A_pB_p}^{(p)}\right]^2, \tag{9.31}$$

where $c_r^{(p)}$ – stiffness coefficient of the rope p,

$\Delta l_{A_pB_p}^{(p)}$ – deformation of the rope p,

$$\delta_r^{(p)} = \begin{cases} 0, & \text{when } \Delta l_{A_pB_p}^{(p)} \le 0 \\ 1, & \text{when } \Delta l_{A_pB_p}^{(p)} > 0 \end{cases}.$$

The derivatives of the potential energy of elastic deformations of the ropes have the form:

$$\frac{V_r^{(p)}}{\partial \mathbf{q}^{(F)}} = -c_r^{(p)} \delta_r^{(p)} \frac{\Delta l_{A_p B_p}^{(p)}}{l_{A_p B_p}^{(p)}} \mathbf{U}_{A_p}^{(F)^T} \bar{\mathbf{r}}_{A_p B_p}^{(p)}, \tag{9.32.1}$$

$$\frac{V_r^{(p)}}{\partial \mathbf{q}^{(L)}} = -c_r^{(p)} \delta_r^{(p)} \frac{\Delta l_{A_p B_p}^{(p)}}{l_{A_p B_p}^{(p)}} \mathbf{U}_{B_p}^{(L)^T} \bar{\mathbf{r}}_{A_p B_p}^{(p)}, \tag{9.32.2}$$

A similar reasoning may be conducted in the case of determining the dependency describing the energy dissipation function:

$$D_r^{(p)} = \sum_{p=1}^{2} \frac{1}{2} b_r^{(p)} \delta_r^{(p)} \left[\Delta \dot{l}_{A_p B_p}^{(p)} \right]^2, \tag{9.33}$$

where $d_r^{(p)}$ – damping coefficients of the rope p.

Hence the formulas:

$$\frac{\partial D_r^{(p)}}{\partial \mathbf{q}^{(F)}} = -b_r^{(p)} \delta_r^{(p)} \mathbf{U}_{A_p}^{(F)^T} \dot{\bar{\mathbf{r}}}_{A_p B_p}^{(p)}, \tag{9.34.1}$$

$$\frac{\partial D_r^{(p)}}{\partial \mathbf{q}^{(L)}} = b_r^{(p)} \delta_r^{(p)} \mathbf{U}_{B_p}^{(L)^T} \dot{\bar{\mathbf{r}}}_{A_p B_p}^{(p)}. \tag{9.34.2}$$

Taking into consideration all components of the Lagrange equations, we obtain the system of differential equations:

$$\mathbf{A}\ddot{\mathbf{q}} = \mathbf{f}(t, \mathbf{q}, \dot{\mathbf{q}}), \tag{9.35}$$

where $\mathbf{A} = \mathbf{A}(t, \mathbf{q})$ – a mass matrix.

In the case when the input in the drive of the travel system has been modelled as force input, equations (9.35) have to be completed by the constrains equations (9.30) and equations of motion have to be presented in the form (9.28). The fourth order Runge-Kutta method has been used to solve the system of equations.

9.1.2 Example of Numerical Calculations

The presented dynamic model of a BOP gantry allows for comprehensive analyses of the device's operation both under usual working conditions and intense waves. Much detailed discussion is contained in the thesis [Urbaś A., 2011].

In the current book, sample results of numerical simulations for phenomena occurring in a gantry's supporting structure are presented. Masses and geometrical parameters of the crane have been chosen based upon technical documentation

(2007). The main parameters are given below: mass of the frame 110 000 kg, mass of the load 550 000 kg, dimension of the load 4,8 m x 5,5 m x 20,3 m. Data concerning the motion of the deck that should be taken into calculation are also provided in the technical documentation (2007) (Table 9.1). In our simulations, the operational conditions have been assumed.

Table 9.1. Deck motion due to waves

Condition	Heading [deg]	Heave [m]	Pitch [rad]	Roll [rad]
Z1	0	0,1343	0,0023	0
Z2	45	0,1115	0,0008	0,0023
Z3	90	0,1140	0	0,0045

Table 9.2. Load cases analysed - gantry crane not moving

Symbol	Description	Clearance	Deck motion
Z1-M0-C0	No clearance in travel system	0	Z1
Z2-M0-C0		0	Z2
Z3-M0-C0		0	Z3
Z1-M0-C1	With clearance in travel system	1cm	Z1
Z2-M0-C1		1cm	Z2
Z3-M0-C1		1cm	Z3

Calculations for the BOP crane that does not move on the deck have been denoted according to the Table 9.2. The same denotations are used in the graphs.

In Fig. 9.9 there are presented time courses of general coordinates $\psi^{(L)}$ of the load of the BOP crane with and without clearance in the travel system.

The influence of clearance in the travel system for the reaction forces in the support system (the leg no. 1) is shown in Fig 9.10. The deck motions Z2 and Z3 are taken into consideration.

The biggest influence of clearance in the travel system on the dynamics of the BOP crane occurs for input Z3, so this input is taken into account for the next calculations. The influence of clearance in the travel system on the reaction forces will be analyzed. The travel velocity is defined by the relation:

$$\begin{aligned} v &= 3at^2 - 4bt^3 \quad \text{when } t \le T_r, \\ v &= v_n \qquad\qquad\ \ \text{when } t > T, \end{aligned} \tag{9.36}$$

where $v_n = 3\dfrac{\text{m}}{\text{min}}$, $T_r = 6\text{sec}$, $a = \dfrac{v_n}{T_r^2}$, $b = \dfrac{v_n}{2T_r^3}$.

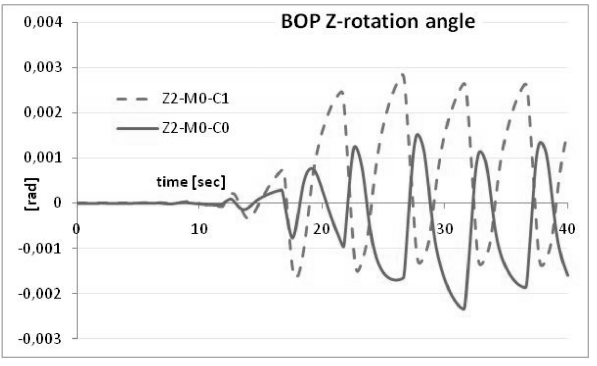

Fig. 9.9. Influence of clearance on roll angle of BOP

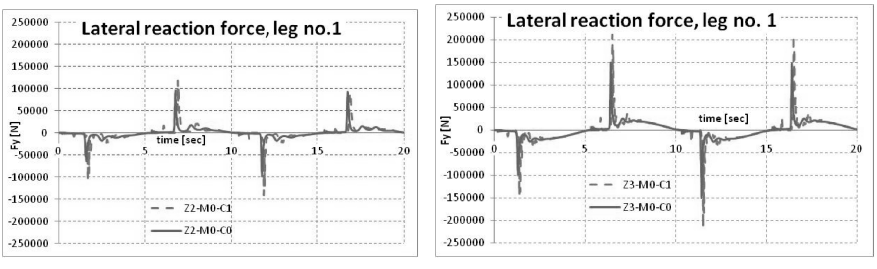

Fig. 9.10. Lateral reaction in leg no.1 (left - in sea conditions Z2, right - in sea conditions Z3)

On the up graph in Fig. 9.11, there is shown the drive force on the first gear (support no. 1) for kinematic and force input and for the case when no clearance occurs in the system. On the bottom graph, there is presented the influence of clearance on the drive force. One can notice that the clearance causes the occurrence of significant dynamic forces of short duration.

Required courses of drive forces acting on the legs 1 and 4 realizing the established travel of the crane are presented in Fig. 9.12. Kinematic and force inputs have been simulated.

The obtained results (values of forces) for assumed parameters are similar, but for kinematic input peak values they are bigger. These values depend on stiffness and damping coefficients taken into account during calculations.

Additional clearance in supporting system for the legs that aren't driven (i. e. 2 and 3), equal to 2 cm, has been taken into consideration, and the results are in Fig 9.13. The obtained values of dynamic forces prove significant influence of clearance on dynamic load of the drive system, the track-way and the whole construction of the crane.

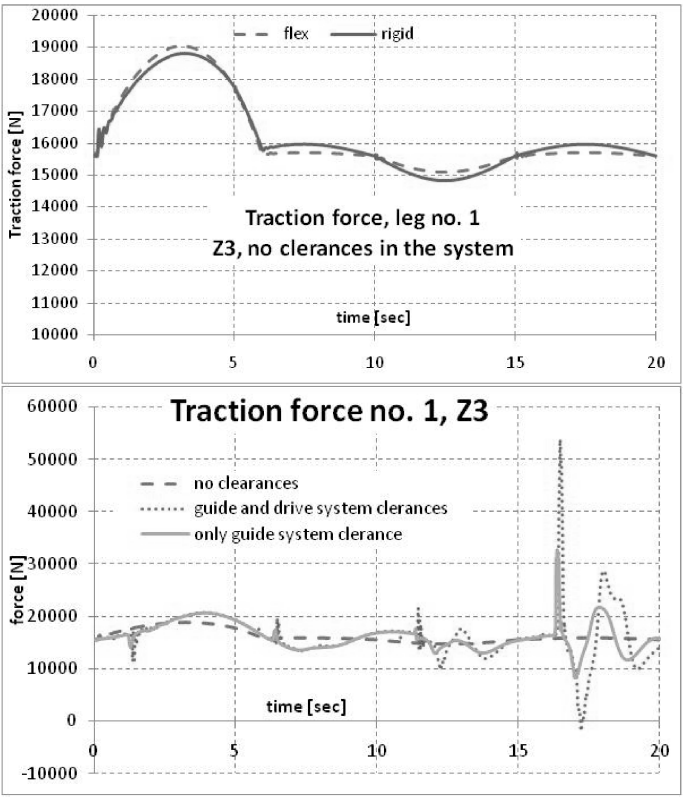

Fig. 9.11. Drive force on gear no. 1 when flexible and rigid model applied (up) influence of different clearances on drive force (bottom)

The mathematical models and the computer programs presented in this section make it possible to execute dynamical analysis of BOP cranes mounted on the floating base. They can be useful in calculating dynamic loads, dimensioning bearing elements of the crane and the track-way. They enable determination of static and dynamic loads by simulation for arbitrarily chosen sea waves conditions.

9.2 Offshore Column Crane with a Shock Absorber

This section discusses a mathematical model of an offshore column crane with a shock absorber [Krukowski J., Maczyński A., 2009], [Krukowski J., Maczyński A., 2010]. As already stated (chapter 2.4.2), in offshore crane design, two kinds of a shock absorber systems are used most commonly. The first one is mounted on

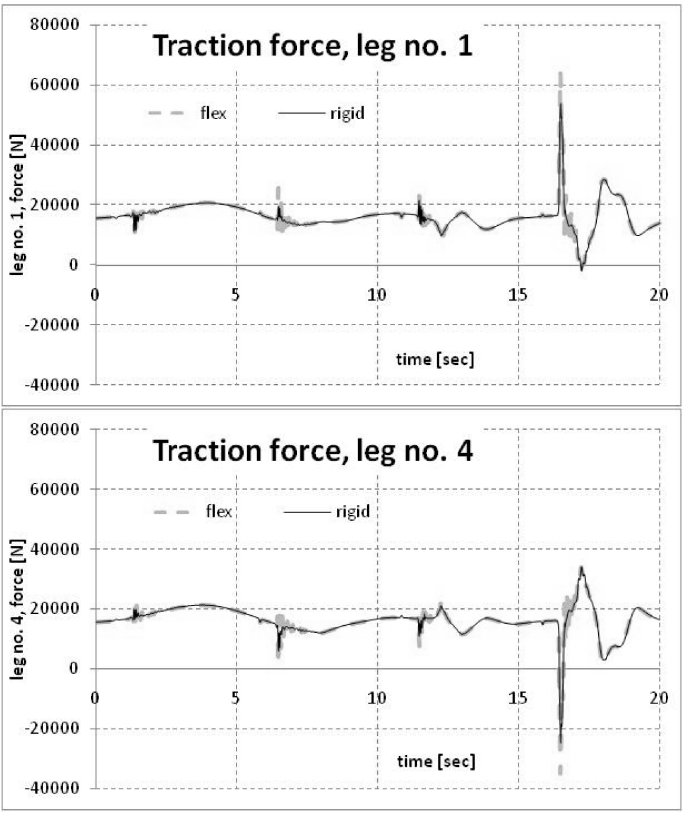

Fig. 9.12. Rigid and flexible drive, leg no. 1 (up) and no. 4 (bottom)

the crane's boom structure. The minimization of dynamic overload is obtained by leading the hoist rope through an additional sliding sheave connected with a hydraulic system. The other one, constituting the system of hydraulic accumulators, is mounted in the hook block.

The subject of the analyses presented in this book is the first type of the shock absorber because of its effectiveness, simple and compact construction. The hydraulic part of the shock absorber is shown in principle in Fig. 2.15. Let us remind that it is the system consisting of accumulator filled with gas and hydraulic cylinder. When force S applied to the piston is big enough, the piston is pulled out and oil is streaming from the cylinder to the accumulator. The end piston stroke length, Δ_2, must normally be shorter than the maximal possible piston stroke length, Δ_{max} minus a safety piston stroke length, Δ_{safe}, to make sure there is no risk for the piston to reach the bottom at normal operation. The safety piston stroke length, Δ_{safe}, shall normally not be less than about 50 mm.

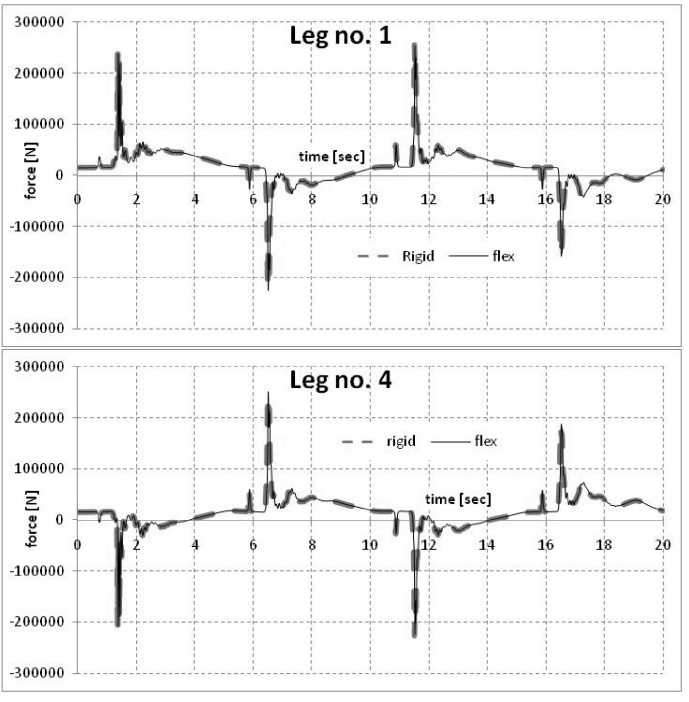

Fig. 9.13. Rigid and flexible drive on legs 1 and 4 - double size clearances in legs 2 and 3

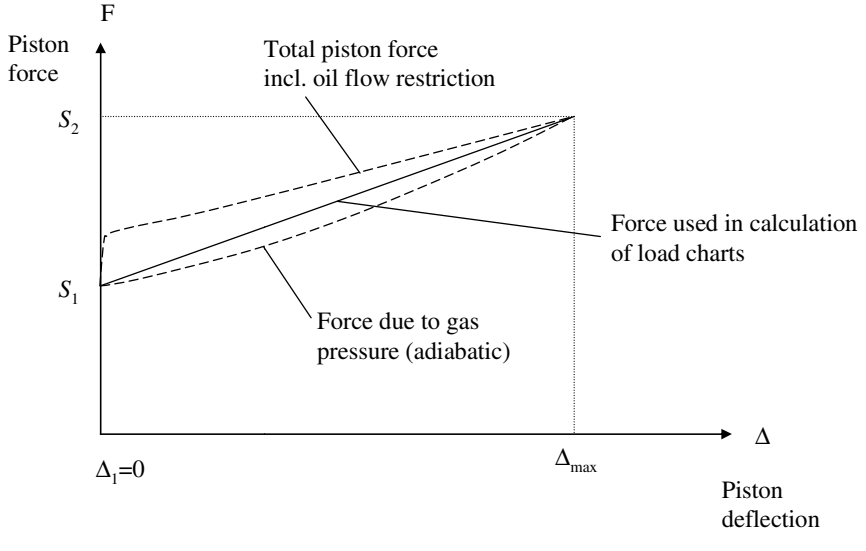

Fig. 9.14. Shock absorber characteristic

The main part of the force *S* on the piston, is balanced by the gas pressure in the accumulator. In addition, there is some oil pressure drop due to restriction when the oil passes the valves between the piston and the accumulator. This is illustrated in Fig. 9.14.

9.2.1 Model of the Offshore Crane

The subject of this section is the offshore pedestal crane equipped with the system reducing dynamic overload, situated on the boom (Fig. 9.15). The analysed crane type is, according to EN 13852-1 Annex L, the "Lattice boom type crane" or API Spec. 2C, type C. The main assumptions adopted at the design stage and the most important connections used during the derivation of equation of motion will be given below. Modelling the shock absorber was particularly emphasised. For the description of the system, joint coordinates and homogenous transformations were used based on Denavit-Hartenberg convention. The equations of motion were obtained using the Rigid Finite Element Method and the Lagrange equations of the second order.

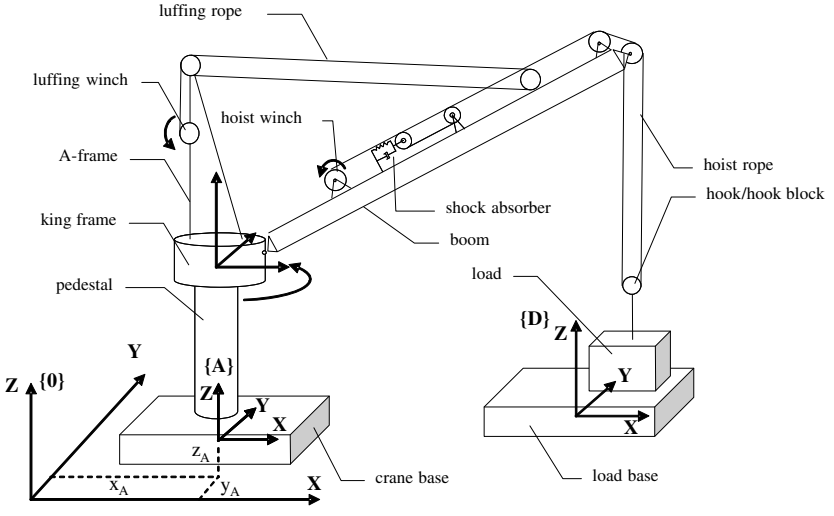

Fig. 9.15. Scheme of an offshore pedestal crane

While preparing the model, the following assumptions and subsystems were taken into consideration:

- the base of the crane (the platform of vessel) is a rigid body with 6 degrees of freedom; the movement is caused by the sea waves defined by pseudo-harmonic functions,

- the pedestal is modelled by means of the Rigid Finite Element Method using a modified approach (MRFEM) – chapter 8.2; hence, the flexibility of the pedestal could be included but also the treatment of the pedestal as a rigid structure is possible,
- the king frame, including the slewing part, is treated as a rigid structure with one degree of freedom with respect to the pedestal – the slew angle,
- the A-frame is modelled by means of MRFEM as a simplified, one-beam system having bending flexibility in the perpendicular direction to the A-frame plane; similarly to pedestal model, the A-frame can be treated as a rigid subsystem,
- the boom is modelled as a continuous system by means of the MFREM,
- the basic element of the shock absorber is the hydraulic cylinder, which is modelled as point mass (additionally including the mass of the moving sheave) connected to the boom by means of a spring damping system; the mass may slide only along the longitudinal axis of the boom; it is assumed that the characteristics of the spring is nonlinear,
- the hoist rope is modelled as a massless element with equivalent longitudinal flexibility; the damping is taken into account, with the assumption it is viscous, and that the damping coefficient has a constant value; with regards to significant changes of the hoist rope during crane operations, the value of rope stiffness coefficient has been made depended on the current rope length,
- the luffing rope is modelled similarly to the hoist rope; as a matter of fact that change of the rope length during crane operations is small, the rope stiffness coefficient is assumed to be constant,
- the load is treated as a material point; its contact with the deck of the supply vessel is taken into account,
- the drive function of the hoist winch can be assumed in two ways: as a kinematic excitation or force excitation by a given moment,
- the luffing winch drive and the slew of the crane has been adopted as a kinematic drive,
- the supply vessel is modelled identical to the crane base.

Modelling of the Crane and Cargo Base Motion

It is assumed that crane base motion and thus movement of the system $\{A\}$ with respect to the system $\{0\}$ is known and described by functions similar to (9.3):

$$y_i^{(A)} = \sum_{j=1}^{n_i^{(A)}} A_{i,j}^{(A)} \sin(\omega_{i,j}^{(A)} t + \varphi_{i,j}^{(A)}); \quad i = 1,...,6, \tag{9.37}$$

where $A_{i,j}^{(A)}, \omega_{i,j}^{(A)}, \varphi_{i,j}^{(A)}$ – respectively: amplitude, phase, frequency and forcing phase angle,

$n_i^{(A)}$ – number of harmonic series.

Movement of the cargo base, i.e. that of system $\{A\}$, will be described in the same way.

In further considerations, the coordinate system $\{0\}$ will be identified with the inertial coordinate system $\{\}$ and the following notation will be used for the homogeneous transformation matrix from coordinate system $\{p\}$ to the coordinate system $\{0\}$:

$$ {}^{0}_{p}\mathbf{T} = \mathbf{T}^{(p)} , \tag{9.38} $$

where p is the number of the member in the kinematic chain.

Homogeneous transformation matrix ${}^{0}_{A}\mathbf{T}$, taking into account the motion of the system $\{A\}$ in $\{\}$, can be presented as a product of six matrices, each being the function of only one variable dependent on time as described in chapter 5. It is to be noticed that if $\tilde{\mathbf{r}} = \begin{bmatrix} \tilde{x} & \tilde{y} & \tilde{z} & 1 \end{bmatrix}^T$ is a vector describing coordinates of the *dm* mass (point) in the local system $\{\}'$, connected to any part of the system, the coordinates of such mass in the system $\{\}$ may be described with the equitation:

$$ \mathbf{r} = {}^{0}_{A}\mathbf{T}(t)\,\overline{\mathbf{T}}(\mathbf{q})\,\mathbf{r}' = \mathbf{T}\,\mathbf{r}' , \tag{9.39} $$

where $\overline{\mathbf{T}}(\mathbf{q}) = {}^{A}_{\{\}'}\mathbf{T}(q_1,\ldots,q_n)$ – transformation matrix of coordinates from local coordinate system $\{\}'$ into the $\{A\}$ coordinate system, dependent on the generalized coordinates $(q_1,\ldots,q_n)$ of the body,

$\mathbf{T} = {}^{0}_{A}\mathbf{T}(t)\overline{\mathbf{T}}(\mathbf{q})$.

Crane Pedestal

As mentioned before, the crane pedestal was discretized by means of MRFEM. The number of rigid finite elements, on which the pedestal was divided, equals n_1+1, where the first rigid finite element of the pedestal, RFE (1,0), is added to the vessel body. The generalized coordinates, describing the location of the second and other rigid elements modelling the pedestal with respect to its predecessors (coordinates describing mutual location of the rigid finite elements some times called flexible or elastic coordinates), may be presented as vectors:

$$ \tilde{\mathbf{q}}^{(1,i)} = \begin{bmatrix} \varphi_x^{(1,i)} & \varphi_y^{(1,i)} & \varphi_z^{(1,i)} \end{bmatrix}^T = \begin{bmatrix} \tilde{q}_x^{(1,i)} & \tilde{q}_y^{(1,i)} & \tilde{q}_z^{(1,i)} \end{bmatrix}^T , \tag{9.40} $$

where $\varphi_x^{(1,i)}$, $\varphi_y^{(1,i)}$, $\varphi_z^{(1,i)}$ are the rotation angles presented in Fig. 9.16.

The vector of generalized coordinates of the RFE yields:

$$ \mathbf{q}^{(1,1)} = \tilde{\mathbf{q}}^{(1,1)} = \begin{bmatrix} q_1^{(1,1)} & q_2^{(1,1)} & q_3^{(1,1)} \end{bmatrix}^T , \tag{9.41.1} $$

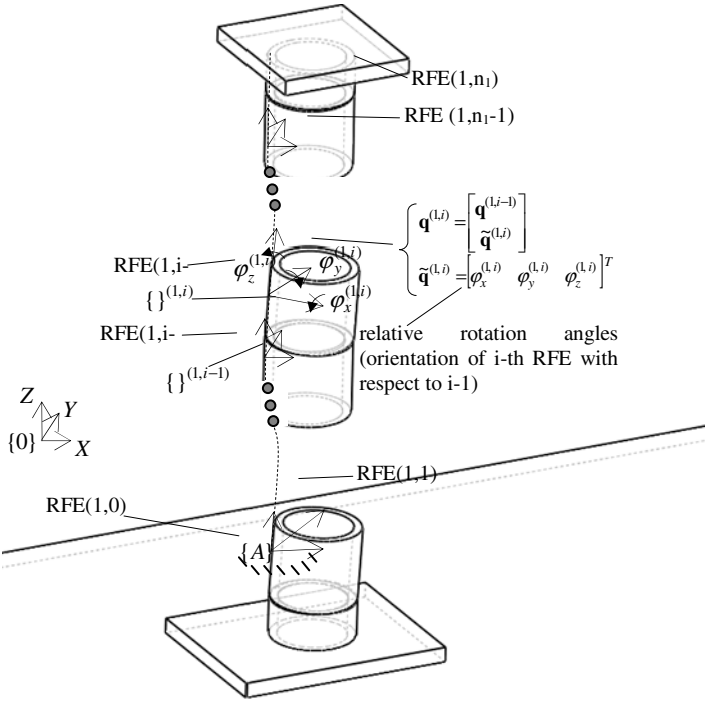

Fig. 9.16. Pedestal discretized by mean of MRFEM

$$\mathbf{q}^{(1,i)} = \begin{bmatrix} \mathbf{q}^{(1,i-1)} \\ \tilde{\mathbf{q}}^{(1,i)} \end{bmatrix} = \begin{bmatrix} q_1^{(1,i)} & q_2^{(1,i)} & \dots & q_{3i}^{(1,i)} \end{bmatrix}^T \quad \text{for } i = 2,..., n_1 . \tag{9.41.2}$$

In accordance to above consideration, during the derivation of the equations of motions, kinetic and potential energy of the RFE (1,0) have been omitted. On the basis of equations presented in previous sections, the kinetic energy of the body discretised by the MRFEM can be calculated as:

$$E_1 = \sum_{i=1}^{n_1} E_{(1,i)} , \tag{9.42}$$

where $E_{(1,i)} = tr\left\{\dot{\mathbf{T}}^{(1,i)}\, \mathbf{H}^{(1,i)}\, \dot{\mathbf{T}}^{(1,i)^T}\right\}$,

$\mathbf{H}^{(1,i)}$ – inertia matrix of the RFE (1,*i*) defined in its own coordinate system,

$\mathbf{T}^{(1,i)}$ – transformation matrix from coordinate system {1,*i*} of RFE (1,*i*) into the coordinate system {},

$$\mathbf{T}^{(1,i)} = \mathbf{T}^{(1,i-1)}\,\tilde{\mathbf{T}}^{(1,i)} = {}^{0}_{A}\mathbf{T}\,\tilde{\mathbf{T}}^{(1,0)}\tilde{\mathbf{T}}^{(1,1)} \cdot \ldots \cdot \tilde{\mathbf{T}}^{(1,i-1)}\,\tilde{\mathbf{T}}^{(1,i)} \quad \text{for } i = 1,..,n_1,$$

$\tilde{\mathbf{T}}^{(1,i)}$ – transformation matrix from coordinate system of RFE (1,i) into coordinate system of RFE (1,i-1).

For the Lagrange equations of the second order, the concept of Lagrange operators is introduced:

$$\varepsilon_i(E) = \frac{d}{dt}\frac{\partial E}{\partial \dot{q}_i} - \frac{\partial E}{\partial q_i}. \tag{9.43}$$

Such operators for other RFE (1,*i*) (*i*=1,...,) of the pedestal, can be written in the vector form as:

$$\boldsymbol{\varepsilon}_{\mathbf{q}^{(1,i)}}\left(E_{(1,i)}\right) == \mathbf{A}^{(1,i)}\ddot{\mathbf{q}}^{(1,i)} + \mathbf{e}^{(1,i)}, \tag{9.44}$$

where $\mathbf{A}^{(1,i)} = \left(a_{k,j}^{(1,i)}\right)_{k,j=1,..,3n_1} = \mathrm{tr}\left\{\mathbf{T}_k^{(1,i)}\,\mathbf{H}^{(1,i)}\,\mathbf{T}_j^{(1,i)T}\right\}$,

$$\mathbf{e}^{(1,i)} = \left(e_k^{(1,i)}\right)_{k=1,...,3n_1} = \sum_{j=1}^{3n_1}\sum_{l=1}^{3n_1}\mathrm{tr}\left\{\mathbf{T}_k^{(1,i)}\,\mathbf{H}^{(1,i)}\mathbf{T}_{j,l}^{(1,i)}\right\}\dot{q}_j^{(1,i)}\,\dot{q}_l^{(1,i)} + $$

$$+\mathrm{tr}\left\{\mathbf{T}_k^{(1,i)}\mathbf{H}^{(1,i)}\left[{}^{0}_{A}\ddot{\mathbf{T}}\,\overline{\mathbf{T}}^{(1,i)} + 2\,{}^{0}_{A}\dot{\mathbf{T}}\,\dot{\overline{\mathbf{T}}}^{(1,i)}\right]^T\right\},$$

$$\overline{\mathbf{T}}^{(1,i)} = \prod_{j=0}^{i}\tilde{\mathbf{T}}^{(1,j)},$$

$$\mathbf{T}_k^{(1,i)} = \frac{\partial \mathbf{T}^{(1,i)}}{\partial q_k^{(1,i)}},$$

$$\mathbf{T}_{j,l}^{(1,i)} = \frac{\partial}{\partial q_j^{(1,i)}}\left(\frac{\partial \mathbf{T}^{(1,i)}}{\partial q_l^{(1,i)}}\right).$$

The potential energy due to gravity forces of the pedestal's rigid finite elements is described by the relation:

$$V_{(1,i)}^{g} = m^{(1,i)}\,g\,\boldsymbol{\theta}_3\mathbf{T}^{(1,i)}\tilde{\mathbf{r}}_C^{(1,i)} \qquad \text{for } i=1,2,...,\ n_1, \tag{9.45}$$

where $m^{(1,i)}$ – mass of the RFE (1,*i*),

$\tilde{\mathbf{r}}_C^{(1,i)}$ – vector of the mass centre of RFE (1,*i*) expressed in its own coordinate system.

The corresponding derivatives, which are the elements of the Lagrange equations, are:

$$\frac{\partial V_{(1,i)}^{g}}{\partial \mathbf{q}^{(1,i)}} = \mathbf{G}^{(1,i)}, \tag{9.46}$$

where $\mathbf{G}^{(1,i)} = \left(g_k^{(1,i)}\right)_{k=1,\ldots,3n_1}$,

$g_k^{(1,i)} = m^{(1,i)} g\, \boldsymbol{\theta}_3 \mathbf{T}_k^{(1,i)} \tilde{\mathbf{r}}_C^{(1,i)}$.

It is known that in MRFEM the successive RFE are connected with each other by means of massless, elasto-damping elements (SDE). Potential energy of the elastic deformation SDE (1,*i*) is defined as follows:

$$V_{(1,i)}^{s} = \frac{1}{2}\left(c_{i,x}^{(1)}\left[\varphi_x^{(1,i)}\right]^2 + c_{i,y}^{(1)}\left[\varphi_y^{(1,i)}\right]^2 + c_{i,z}^{(1)}\left[\varphi_z^{(1,i)}\right]^2 \right) = \frac{1}{2}\sum_{j=1}^{3} c_{i,j}^{(1)}\left[\tilde{q}_j^{(1,i)}\right]^2, \tag{9.47}$$

where $c_{i,x}^{(1)} = c_{i,1}^{(1)}$, $c_{i,y}^{(1)} = c_{i,2}^{(1)}$, $c_{i,z}^{(1)} = c_{i,3}^{(1)}$ where the adequate coefficients of the rotational stiffness of SDE (1,*i*).

Equation (9.47) can be presented in the form:

$$V_{(1,i)}^{s} = \frac{1}{2}\tilde{\mathbf{q}}^{(1,i)^T}\mathbf{C}^{(1,i)}\tilde{\mathbf{q}}^{(1,i)}, \tag{9.48}$$

where $\mathbf{C}^{(1,i)} = \begin{bmatrix} c_{i,1}^{(1)} & 0 & 0 \\ 0 & c_{i,2}^{(1)} & 0 \\ 0 & 0 & c_{i,3}^{(1)} \end{bmatrix}$.

The required derivatives of the potential energy of elastic deformation with respect to generalized coordinates $\tilde{\mathbf{q}}^{(1,i)}$, have a simple form:

$$\frac{\partial V_{(1,i)}^{s}}{\partial \tilde{\mathbf{q}}^{(1,i)}} = \mathbf{C}^{(1,i)}\tilde{\mathbf{q}}^{(1,i)}. \tag{9.49}$$

It may additionally be assumed that in SDE (1,*i*) dissipation of the energy appears, which is described by means of equations:

$$D_{(1,i)} = \frac{1}{2}\left(b_{i,x}^{(1)}\left[\dot{\varphi}_x^{(1,i)}\right]^2 + b_{i,y}^{(1)}\left[\dot{\varphi}_y^{(1,i)}\right]^2 + b_{1,z}^{(1)}\left[\dot{\varphi}_z^{(1,i)}\right]^2 \right) = \frac{1}{2}\sum_{j=1}^{3} b_{1,j}^{(1)}\left[\dot{\tilde{q}}_j^{(1,i)}\right]^2, \tag{9.50}$$

where $b_{i,x}^{(1)} = b_{i,1}^{(1)}$, $b_{i,y}^{(1)} = b_{i,2}^{(1)}$, $b_{i,z}^{(1)} = b_{i,3}^{(1)}$ are respective damping coefficients of the SDE (1,*i*).

Equation (9.50) may be also written as:

$$D_{(1,i)} = \frac{1}{2}\dot{\tilde{\mathbf{q}}}^{(1,i)T}\mathbf{B}^{(1,i)}\dot{\tilde{\mathbf{q}}}^{(1,i)}, \tag{9.51}$$

where $\mathbf{B}^{(1,i)} = \begin{bmatrix} b_{i,1}^{(1)} & 0 & 0 \\ 0 & b_{i,2}^{(1)} & 0 \\ 0 & 0 & b_{i,3}^{(1)} \end{bmatrix}$,

and the adequate derivatives can be obtained from:

$$\frac{\partial D_{(1,i)}}{\partial \dot{\tilde{\mathbf{q}}}^{(1,i)}} = \mathbf{B}^{(1,i)}\dot{\tilde{\mathbf{q}}}^{(1,i)}. \tag{9.52}$$

King Frame/Slewing Part

Let us define the following vector of generalized coordinates for the slewing part:

$$\mathbf{q}^{(2)} = \begin{bmatrix} \mathbf{q}^{(1,n_1)} \\ \varphi_z^{(2)} \end{bmatrix} = \begin{bmatrix} q_1^{(2)} & q_2^{(2)} & \dots & q_{n_2}^{(2)} \end{bmatrix}^T, \tag{9.53}$$

where $\varphi_z^{(2)}$ symbolizes the angle of rotation of the slewing part with respect to the pedestal.

The kinetic energy of the slewing part can be described as:

$$E_2 = tr\left\{\dot{\mathbf{T}}^{(2)}\,\mathbf{H}^{(2)}\,\dot{\mathbf{T}}^{(2)^T}\right\}, \tag{9.54}$$

where $\mathbf{H}^{(2)}$ – the inertial matrix of the slewing part.

Lagrange operators for the slewing part are formulated in the form:

$$\boldsymbol{\varepsilon}_{\mathbf{q}^{(2)}}(E_2) = \mathbf{A}^{(2)}\ddot{\mathbf{q}}^{(2)} + \mathbf{e}^{(2)}, \tag{9.55}$$

where $\mathbf{A}^{(2)} = \left(a_{i,l}^{(2)}\right)_{i,l=1,\dots,n_2} = \mathrm{tr}\left\{\mathbf{T}_i^{(2)}\,\mathbf{H}^{(2)}\,\mathbf{T}_l^{(2)T}\right\}$,

$$\mathbf{e}^{(2)} = \left(e_i^{(2)}\right)_{i=1,\dots,n_2} = \mathrm{tr}\left\{\mathbf{T}_i^{(2)}\,\mathbf{H}^{(2)}\left[{}_A^0\ddot{\mathbf{T}}\,\overline{\mathbf{T}}^{(2)} + 2\,{}_A^0\dot{\mathbf{T}}\sum_{j=1}^{n_2}\overline{\mathbf{T}}_j^{(2)}\,\dot{q}_j^{(2)} + \right.\right.$$

$$\left.\left. + \sum_{l=1}^{n_2}\sum_{j=l}^{n_2}\delta_{l,j}\,\mathbf{T}_{l,j}^{(2)}\,\dot{q}_l^{(2)}\,\dot{q}_j^{(2)}\right]^T\right\},$$

$$\delta_{l,j} = \begin{cases} 1 & \text{for} \quad l = j \\ 2 & \text{for} \quad l \neq j \end{cases},$$

$$\overline{\mathbf{T}}^{(2)} = \tilde{\mathbf{T}}^{(1,0)}\, \tilde{\mathbf{T}}^{(1,1)} \cdot \ldots \cdot \tilde{\mathbf{T}}^{(1,n_1)} \cdot {}^{(1,n_1)}_{2}\mathbf{T},$$

${}^{(1,n_1)}_{2}\mathbf{T}\left(\varphi_z^{(2)}\right)$ – the transformation matrix form coordinate system of slewing part {2} to the last rfe coordinate system of pedestal $\{1,n_1\}$.

Potential energy of the gravity forces of the slewing body equals:

$$V_2^g = m^{(2)} g\, \boldsymbol{\theta}_3 \mathbf{T}^{(2)} \tilde{\mathbf{r}}_C^{(2)}, \tag{9.56}$$

where $m^{(2)}$ – mass of the slewing part,

$\tilde{\mathbf{r}}_C^{(2)}$ – position vector of the center of slewing part mass, expressed in the system {2}.

The necessary derivatives are defined bellow:

$$\frac{\partial V_2^g}{\partial \mathbf{q}^{(2)}} = \mathbf{G}^{(2)}, \tag{9.57}$$

where $\mathbf{G}^{(2)} = \left(g_k^{(2)}\right)_{k=1,\ldots,n_2}$,

$g_k^{(2)} = m^{(2)} g\, \boldsymbol{\theta}_3 \mathbf{T}_k^{(2)} \tilde{\mathbf{r}}_C^{(2)}$.

A-Frame and Boom

As mentioned above, the A-frame is modelled by means of the MRFEM in compliance with only bending flexibility in the perpendicular direction to the plane of the A-frame. Additionally, as for the pedestal, RFE (3,0) is added to the slewing part, and as a result, it does not have its own generalized coordinates (Fig. 9.17). Consequently, the following vectors of generalized coordinates for each rfe of the A-frame are defined:

- one-element vectors of the flexible coordinates:

$$\tilde{\mathbf{q}}^{(3,1)} = \left[\varphi_y^{(3,1)}\right]; \ldots; \tilde{\mathbf{q}}^{(3,n_3)} = \left[\varphi_y^{(3,n_3)}\right], \tag{9.58}$$

- coordinate vectors describing position of the rigid element with respect to the base coordinate system:

$$\mathbf{q}^{(3,i)} = \left[\mathbf{q}^{(2)} \quad \tilde{\mathbf{q}}^{(3,1)} \quad \ldots \quad \tilde{\mathbf{q}}^{(3,i)}\right]^T = \left[q_1^{(3,i)} \quad \ldots \quad q_{n_2+i}^{(3,i)}\right]^T \quad \text{for } i=1,2,\ldots,\ n_3. \tag{9.59}$$

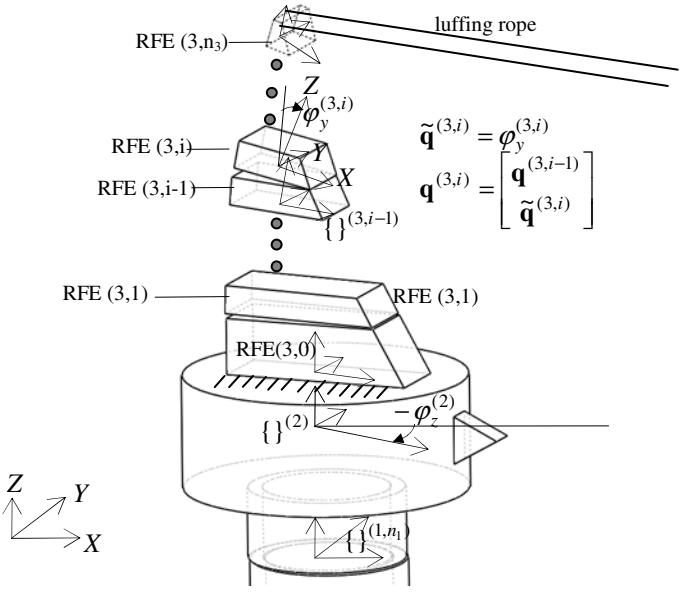

Fig. 9.17. Simplified model of flexible A-frame

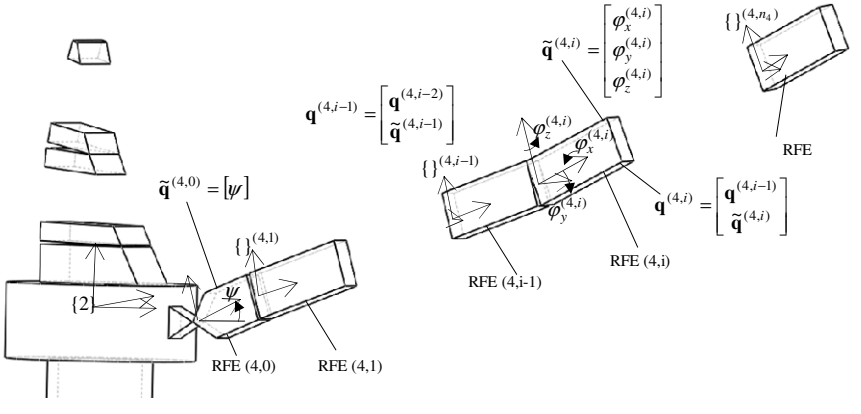

Fig. 9.18. Flexible boom discretized by mean of the MRFEM

In contrast to the pedestal and A-frame, in the case of boom it was assumed that there is a rotational connection defined by the boom angle ψ between the rotating part {2} and the RFE (4,0) (Fig 9.18). We can define the following vectors of generalized coordinates for the boom:

- vectors of the rigid and flexible coordinates:

$$\tilde{\mathbf{q}}^{(4,0)} = [\psi] = \left[\varphi_y^{(4,0)}\right]; \ldots; \tilde{\mathbf{q}}^{(4,i)} = \left[\varphi_x^{(4,i)} \quad \varphi_y^{(4,i)} \quad \varphi_z^{(4,i)}\right]^T \text{ for } i=1,2,\ldots, n_4, \quad (9.60)$$

- coordinate vectors describing position of the rigid element with respect to the base coordinate system:

$$\mathbf{q}^{(4,i)} = \left[\mathbf{q}^{(2)^T} \quad \tilde{\mathbf{q}}^{(4,0)^T} \quad \ldots \quad \tilde{\mathbf{q}}^{(4,i)^T}\right]^T = \left[q_1^{(4,i)} \quad \ldots \quad q_{3i+n_2+1}^{(4,i)}\right]^T \text{ for } i=0,1,\ldots, n_4 . \quad (9.61)$$

The necessary elements of the Lagrange equations related to the A-frame and boom subsystems were calculated in the same way as presented for the crane pedestal.

The Model of Shock Absorber

The model of shock absorber is presented in Fig. 9.19. Its basic element is sheave (3) possessing the mass m_{sA} mounted to the boom by means of a parallel spring-damping system. Relative motion of the sheave (3) is possible only along the longitudinal axis of the boom. The mass m_{sA} is enlarged due to movable parts of the hydraulic cylinder.

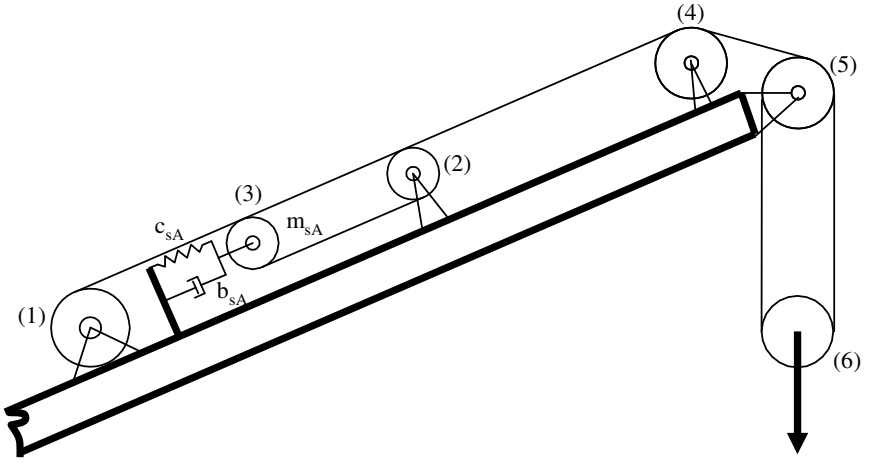

Fig. 9.19. Model of the shock absorber

The shock absorber is activated only if the hoist rope tension reaches specific value (and does not exceed design limits). Usually, in practical hand calculations, one assumes a multilinear characteristic (Fig. 9.14), but its first derivative is not determinable in points defining the working range. This is unfavourable in numerical simulations.

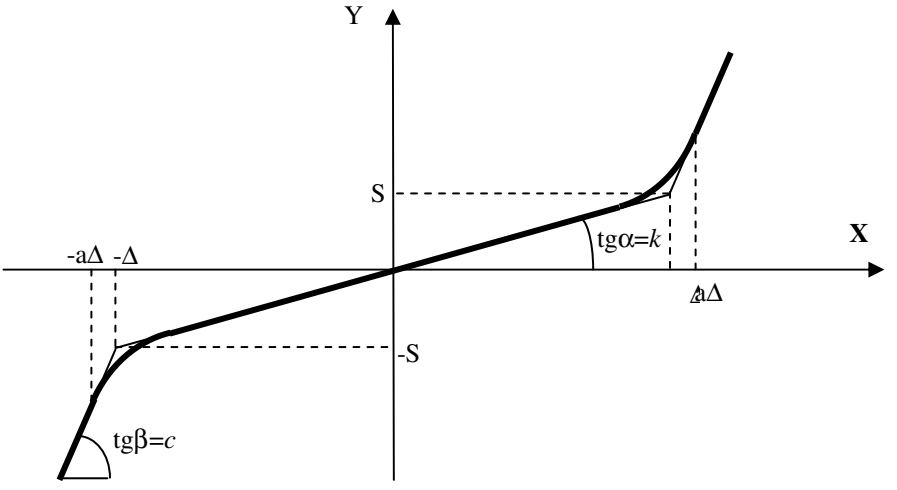

Fig. 9.20. Characteristic of an elastic element $c_{sA}=c_{sA}(x)$

In the presented model, characteristic shown in Fig. 9.20 was assumed [Krukowski J., Maczyński A., 2011]. It represents the characteristic of elastic element $c_{sA}=c_{sA}(x)$, and does not take into account the situation when the shock absorber sheave (3) is fixed to the boom structure. The curve given in Fig. 9.20 can be described as follow:

$$y=\begin{cases} S+c(x-\Delta) & \text{for} \quad x \geq a\Delta \\ kx+\alpha x^2 e^{\beta x} & \text{for} \quad 0 \leq x < a\Delta \\ -S+c(x-\Delta) & \text{for} \quad x \leq -a\Delta \\ kx-\alpha x^2 e^{-\beta x} & \text{for} \quad -a\Delta < x < 0 \end{cases}. \tag{9.62}$$

By selecting appropriate values of α and β, one obtains a smooth transition curves at the point $x = a\Delta$ (and $x = -a\Delta$). Then, the following conditions must be fulfilled:

$$ka\Delta+\alpha(a\Delta)^2 e^{\beta a\Delta}=S+c(a\Delta-\Delta)=k\Delta+c(a-1)\Delta, \tag{9.63.1}$$

$$k+2\alpha a\Delta e^{\beta a\Delta}+\alpha a^2\Delta^2\beta e^{\beta a\Delta}=c. \tag{9.63.2}$$

After some transformation, parameters α and β are obtained:

$$\beta=\frac{2-a}{a\Delta(a-1)}, \tag{9.64.1}$$

$$\alpha=\sqrt{\frac{(a-1)(c-k)}{a^2\Delta e^{\beta a\Delta}}}. \tag{9.64.2}$$

The shock absorber is designed in such a way that it works only under the tensioning load. Up to the value of force S_1, the stiffness has a very high value. Within the limit of forces S_1 to S_2, the stiffness decreases (shock absorber working range), and beyond force S_2 the stiffness increases significantly. The characteristic of an elastic element from Fig. 9.20 must be appropriately scaled to the form shown in Fig. 9.21.

Shock absorber working parameters are defined by the following variables:

S_1, S_2 – minimum/maximum force from which shock absorber is active,

Δ_1, Δ_2 – displacement of the shock absorber sheave corresponding to the force S_1, S_2,

a – parameter specifying where the point of curvilinear part of characteristic is becoming rectilinear, $\alpha > 1$,

α, β – parameters defining the shape of the characteristic described in equation (9.64).

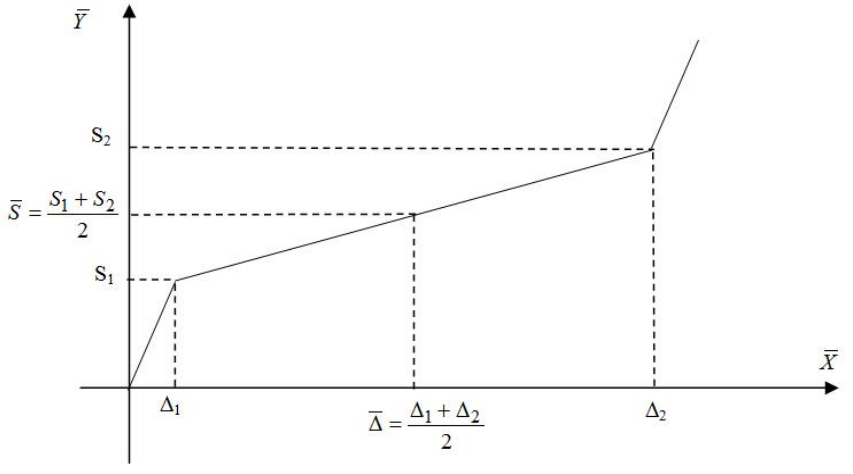

Fig. 9.21. Characteristic of shock absorber

From Fig. 9.21 it is easy to read, that the constans c and k are described by means of:

$$c = \frac{S_1}{\Delta_1}, \tag{9.65.1}$$

$$k = \frac{S_2 - S_1}{\Delta_2 - \Delta_1}, \tag{9.65.2}$$

and the values of x and y are determined as:

$$\begin{cases} y = \bar{y} - \bar{S} \\ x = \bar{x} - \bar{\Delta} \end{cases}. \tag{9.66}$$

where $\bar{x}$, $\bar{y}$, $\bar{\Delta}$ and $\bar{S}$ are shown in Fig. 9.21.

Hoisting and Luffing Ropes

The potential energy of elastic deformation and function of dissipation energy of the hoist rope and luffing rope can be described by the following equations:

$$V_l = \frac{1}{2}\delta c^{(l)} \Delta_l^2, \tag{9.67}$$

$$D_l = \frac{1}{2}\delta b^{(l)} \dot{\Delta}_l^2, \tag{9.68}$$

where $\delta = \begin{cases} 0 & \text{for } \Delta_l \le 0 \\ 1 & \text{for } \Delta_l > 0 \end{cases}$,

Δ_l – elongation of the hoist rope or luffing rope,

$c^{(l)}, b^{(l)}$ – stiffness and damping coefficients of rope, respectively.

Because of the possibility of the significant changes in the active length of the hoist rope during crane operation, the stiffness coefficient of the hoist rope is determining by means of:

$$c^{(l)} = \frac{E_6 F_6}{L_{6,0} - \alpha_{(6)} r_{(6)}}, \tag{9.69}$$

where $L_{6,0}$ – the initial length of hoist rope,

E_6 – Young's modulus of the wire rope core,

F_6 – cross section of the wire rope,

$\alpha_{(6)}$ – rotation angle of the hoist winch drum,

$r_{(6)}$ – radius of the hoist winch drum.

The stiffness coefficient $c^{(l)}$ of the luffing rope is considered as a constant value. A method for determining the necessary derivatives of equations (9.67) and (9.68) was described in chapter 9.1.

Load

The load was modelled as a material point. The weight of the hook block was added to the weight of the load. The vector of the generalized coordinates is defined as:

$$\mathbf{q}^{(L)} = \left[x^{(L)} \quad y^{(L)} \quad z^{(L)}\right]^T = \left[q_1^{(L)} \quad q_2^{(L)} \quad q_3^{(L)}\right]^T. \tag{9.70}$$

The kinetic and potential energy of the load are described by means of:

$$E_L = \frac{1}{2} m^{(L)} \left(\dot{x}^{(L)2} + \dot{y}^{(L)2} + \dot{z}^{(L)2} \right), \tag{9.71}$$

$$V_L^g = m^{(L)}\ g\ z^{(L)}\ , \tag{9.72}$$

where $m^{(L)}$ is the mass of the load.

On this basis, it is possible to write:

$$\boldsymbol{\varepsilon}_{\mathbf{q}^{(L)}} = \mathbf{A}^{(L)} \cdot \ddot{\mathbf{q}}^{(L)}, \tag{9.73}$$

$$\frac{\partial V_L^g}{\partial \mathbf{q}^{(L)}} = \left[0 \quad 0 \quad m^{(L)} g\right]^T, \tag{9.74}$$

where $\mathbf{A}^{(L)} = diag\left[m^{(L)}, m^{(L)}, m^{(L)}\right]$.

The developed computer software allows us to simulate the following cases:

1. load is in the air (water) – does not remain in contact with the deck of a supply vessel,
2. load remains stationary on board of the supply vessel; its coordinates are defined by the motion of the supply vessel,
3. load can by frozen to the deck, or other reason cause that the load is permanently connected to the supply vessel.

Drive Systems

Slewing, hoisting and luffing drive systems are modelled as the kinematic inputs. Therefore, the following function is known:

$$\phi_d = \phi_d(t), \tag{9.75}$$

where ϕ_d is respectively: slewing angle, hosting winch or luffing winch rotation angle.

From the perspective of planned applications of the presented model, the hosting machinery is one of the most significant drive system. Therefore, a second method of its modelling, using the force excitation, has been developed. Based on the analysis of literature (for example [Osiński M. et al., 2004]) as well as experience acquired from crane operators and designers, the hoist winch characteristic was assumed as shown in Fig. 9.22.

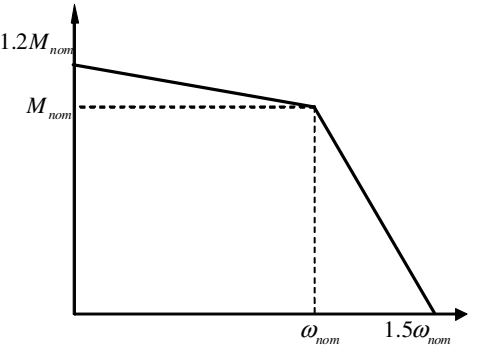

Fig. 9.22. Hoist winch characteristic

Agregation of the Equations of Motion

The equations of motion of the whole crane can be written as:

$$\mathbf{A}\,\ddot{\mathbf{q}} = \mathbf{F}\ , \tag{9.76}$$

where $\mathbf{A}$ – mass matrix,
$\mathbf{q}$ – vector of generalized coordinates,
$\mathbf{F}$ – the right side vector; its elements are designated as the partial derivatives of the kinetic energy, potential forces of gravity and flexibility, partial derivatives of function of dissipation energy and units derived from external forces.

The equations (9.76) were solved by a computer program using the fourth order of the Runge-Kutta method with fixed step integration. Before the integration of (9.76), initial conditions were calculated by solving the above equations assuming $\ddot{\mathbf{q}} = \dot{\mathbf{q}} = \mathbf{0}$. The resulting system of nonlinear algebraic equations was solved using the Newton's method.

9.2.2 Examples of Numerical Calculations

Example of simulation results obtained from the developed computer programme are presented in this section. Two load cases are considered:

LC-1: Hoisting of the load from a stationary deck.

LC-2: Hoisting from the deck which movement is described by the function:

$$z_P = 0.75\sin\left(\frac{2\pi}{6}t\right)\,[\mathrm{m}]. \tag{9.77}$$

A load of 18000 kg (including wire rope and hook block mass) is lifted from a supply boat deck. Assuming that the wire rope is loose at the beginning of the cycle (by a length of 1 m), some dynamic overload can be expected. The hoisting speed is assumed 0.4 m/s for quadruple operation, with the drum rotation characteristics consistent with Fig. 9.22. The shock absorber was defined by the following parameters: $S_1 = 97\ 5\,00$ N, $S_2 = 1.4 S_1$, $\Delta_1 = 0.02$ m, $\Delta_2 = 0.52$ m, $a = 1.1$.

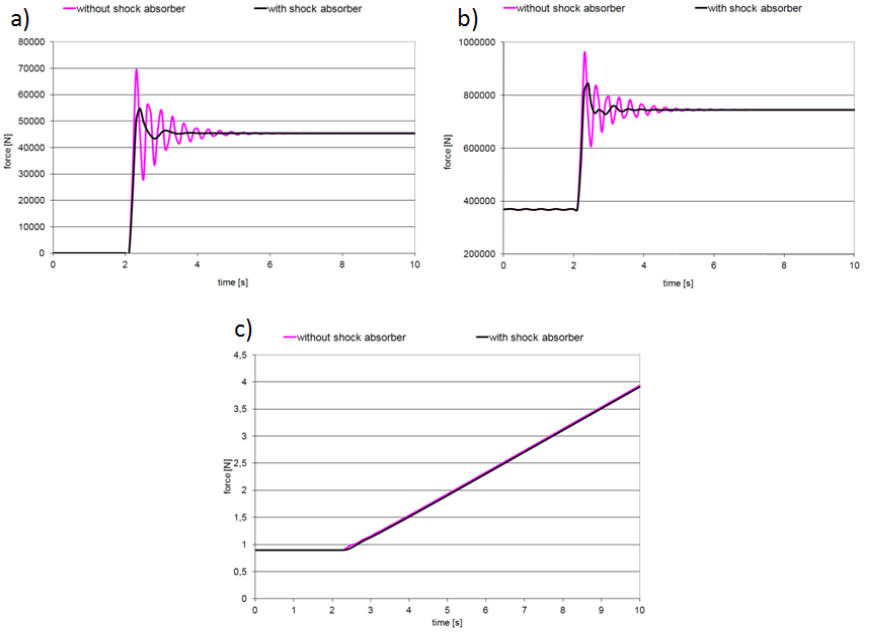

Fig. 9.23. LC-1 load case results: a) hoist rope force, b) luffing rope force,c) z coordinate of the load

In Fig. 9.23, there are presented time courses of the main hoist wire tension force, luffing wire force and z-coordinate of the load during lifting operation. Two crane models: working with and without shock absorber, are compared. The whole crane structure was assumed rigid.

The conditions assumed in the presented examples are rather theoretical – the winch acceleration during the first phase (when the rope is loose) produces a high dynamic peak load when the wire is suddenly pre-tensioned. This is one of the reason why a DAF (dynamic amplification factor) is applied when selecting various crane components. However, this scenario is simulated in order to show how effective the shock absorber could be. Even if the operator runs, be mistake, the winch without load (or there could be an imperfection in a drive system), thanks to the automatic overload protection system dynamic load in the hoist rope

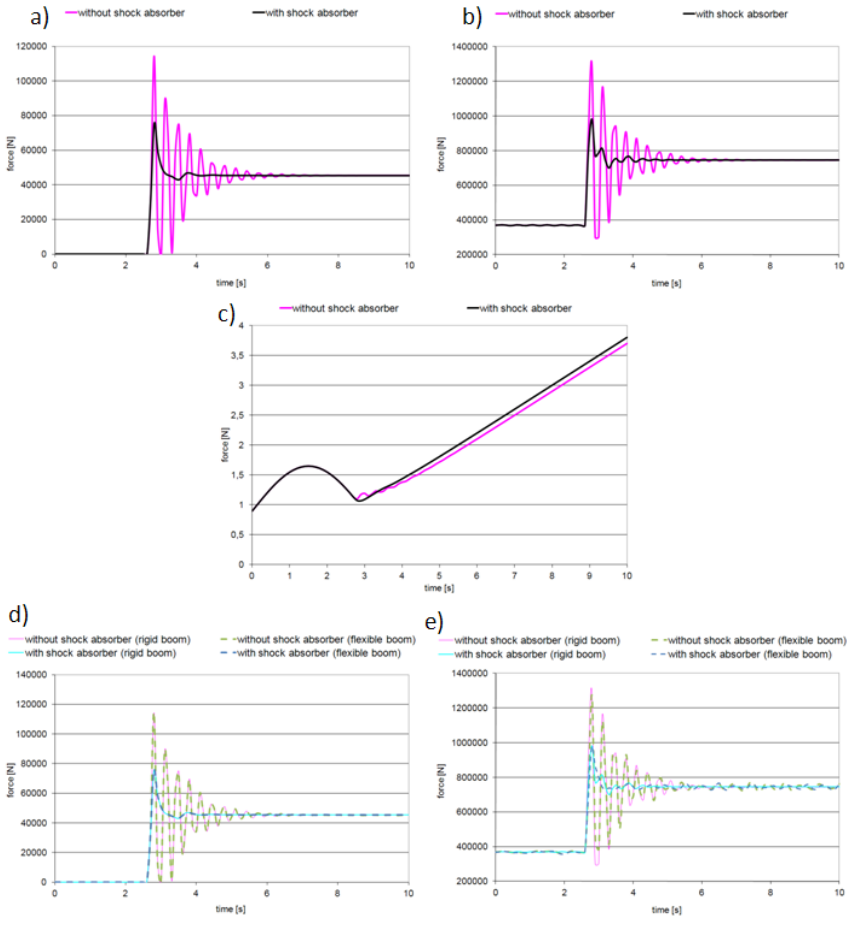

Fig. 9.24. LC-2 load case results: a) hoist rope force, b) luffing rope force, c) z coordinate of the load, d) hoist rope force (rigid and flexible crane jib), e) luffing rope force (rigid and flexible crane jib)

is reduced by approximately 100%. In some cases, without such a systems, the tension can be close to the breaking load of the wire, which if not breaks it at the accident time, makes its life time much shorter.

The plots shown in Fig. 9.24 were obtained for the load case LC-2. The results for the rigid crane gantry was compared with those obtained with flexible structure. Discretisation of the crane boom was performed using $n_4 = 7$ rigid finite elements.

The results of numerical simulations performed using the crane model having shock absorber installed confirm a significant decrease of dynamic overload experienced by the structural systems. Application of the shock absorber subsystem in real constructions would allow the crane to work in much more difficult conditions. Without such a systems, the same crane has to be de-rated, which makes it in a higher sea state less efficient handling tool, causing that the

whole vessel or platform can not perform planned lifts, until the weather conditions improve. Consequently, the load chart of a crane equipped with an overload protection system will be much more different than the same construction without such a control device. Therefore, properly working shock absorber is now a relatively new technique in the offshore industry.

Taking into consideration flexibility of the boom does not significantly change the obtained results. Some slight differences are observed in the time history of the luffing rope force. It therefore appears that, for the preliminary calculations or for the bids purpose, the flexibility of the boom can be omitted. On the basis of a model with few degrees of freedom, an engineer obtains a quick software tool, supporting him during the design process. The calculation model presented enable us to determine the crane overload in various working conditions. That makes it possible to predict limiting weather conditions for a given crane design and specific operation scenarios. Implementation of the model in a standalone desktop application makes it attractive for various conceptual ad-hoc analyses.

9.3 Laying of Pipelines

The methods of analysing multibody systems, models of connections and materials presented in previous chapters were implemented in software suited for static and dynamic analyses of the installation process of pipelines for transporting oil and gas, of transfer lines (cables) and other types of infrastructure related to exploiting deposits of the seabeds. The current section discusses models operations commonly performed in reality. The constructed models and software are also indirectly verified. For this purpose, additional models in the ANSYS package are formulated and the results of calculations compared. Detailed derivations and a description of those models are offered in [Szczotka M., 2011b].

The Programme Pipelaysim

Based on the presented models, a computer programme supporting static and dynamic analysis of basic operations related to installing pipes. The programme is written in the C++ language (*Microsoft Visual Studio 2008* IDE), using elements of the *Delphi* package which are parts of *Borland Developer Studio 2006*. To produce graphics Silicon Graphics Inc's *OpenGL* library is used.

The main window of the programme *PipeLaySim* is shown in Fig. 9.25. It acts as a preprocessor. The user can, by means of standard interface components (GUI), define (or load from an external file) any parameters of the models and analysis options. In the main panel of the programme there are buttons assembled which enable running subsequent simulations for supported installation methods.

Results obtained from the calculations may be analysed in a built-in module for creating graphs or exported as text files and further processed in other programmes (e.g. in Excel). A functionality which may be found useful is passing the results of calculations in the form of scripts to the engineering computation system MATLAB. The software also supports concurrently displaying an

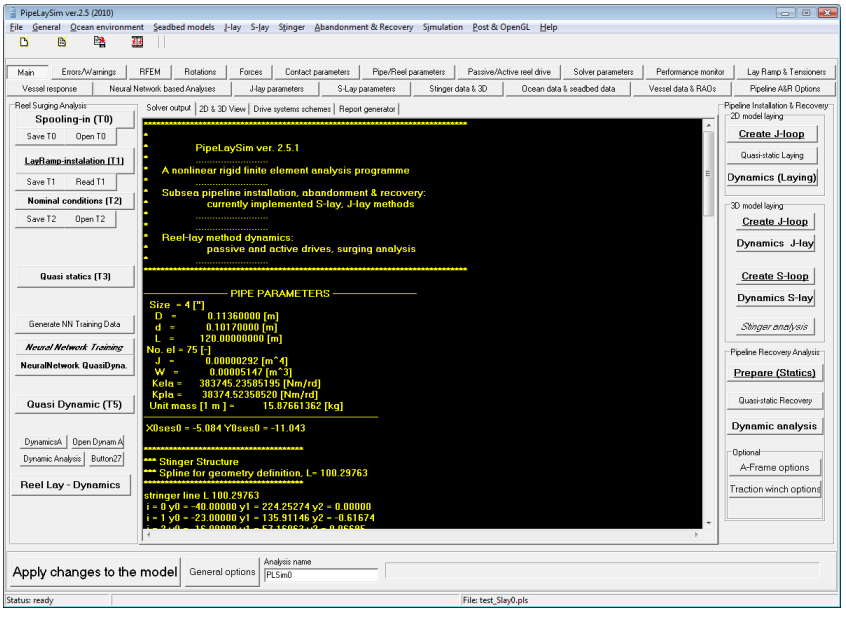

Fig. 9.25. Main window of the programme *PipeLaySim*

animation of the simulated system and saving it to multimedia files (for example *.avi). Sample postprocessor window with an animation produced using the *OpenGL* libraries is shown in Fig. 9.26.

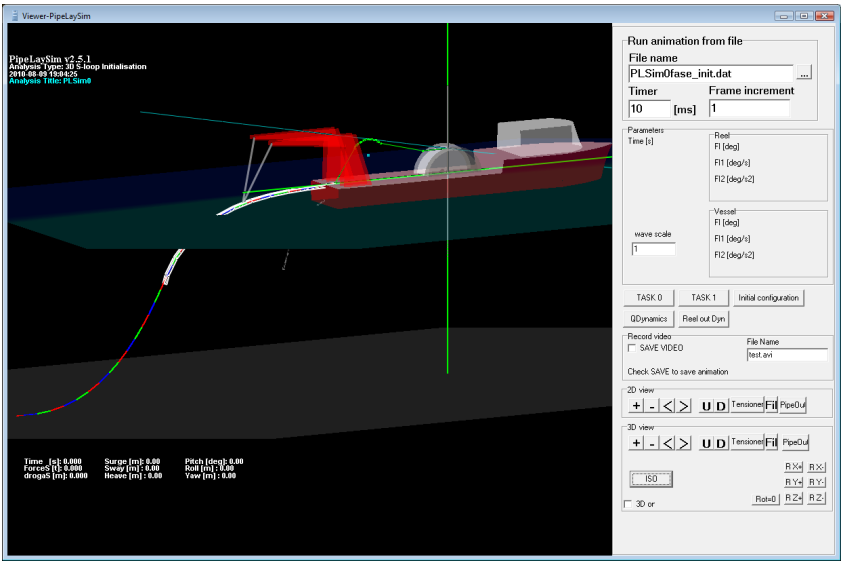

Fig. 9.26. Sample animation window in the programme *PipeLaySim*

9.3.1 Mathematical Model of the J-Lay Method

For the model used to simulate an installation process with the J-lay method (Fig. 9.27) the pipeline is assumed to be ejected from a guiding ramp whose inclination angle relative to the deck is $\alpha_T = const$. It is further assumed that RFE 0 is ejected with a known velocity $v_T(t)$ of laying which corresponds to the vessel's velocity. Because of the lifting movements caused by waves, the pipeline is subjected to forces due to the difference of velocities of laying and of the point *S*. In addition to that, hydrodynamic forces caused by waves and sea currents act on the pipeline. A detailed derivation of the equations of motion for the considered system can be obtained by using the dependencies from previous chapters. Therefore below only selected formulas related to modelling constraints imposed on the pipeline are given.

Equations of constraints related to the connection of the RFE 0 with the base by a spherical joint at the point *H* and the reactions $\mathbf{P}^{(0)}$ may be introduced into the system directly by using the dependencies for a spherical joint. The components of the reaction $\mathbf{P}^{(0)}$ in the system $\{\}_A$ may be calculated from the formula:

$$\tilde{\mathbf{P}}_A^{(0)} = \mathbf{R}_A^T \mathbf{P}^{(0)}, \tag{9.78}$$

where $\mathbf{R}_A$ – rotation matrix of the system $\{\}_A$ relative to $\{\}$,

$\tilde{\mathbf{P}}_A^{(0)}$ – reaction vector at the point *H* expressed in $\{\}_A$,

$\mathbf{P}^{(0)}$ – reaction vector at the point *H* expressed in the system $\{\}$.

The RFE with number *n* is placed in the ramp's guide. As the pipeline is ejected from the guide, the length of the segment off the vessel increases. When RFEs of constant length are used, incrementing the number n_{SES} (of RFEs and SDE in the system) is necessary. The general form of constraint equations imposed on the RFE *n* is:

$$\begin{aligned} \tilde{\mathbf{r}}_s &= \tilde{\mathbf{r}}_n + \tilde{\mathbf{R}}_n \tilde{\mathbf{r}}_s' = \tilde{\mathbf{a}}_s \\ \tilde{\mathbf{\Phi}}_n &= \tilde{\mathbf{\Lambda}}_s \end{aligned}, \tag{9.79}$$

where $\tilde{\mathbf{a}}_s = const$ – vector describing the position of the point *S* in $\{\}_A$,

$\tilde{\mathbf{\Lambda}}_s = const$ – vector describing the orientation of the guide in $\{\}_A$,

$\tilde{\mathbf{r}}_s' = \tilde{\mathbf{r}}_s'(t)$ – vector describing the coordinates of the point *S* in the system $\{\}_n$,

$\tilde{\mathbf{r}}_n, \tilde{\mathbf{\Phi}}_n$ – components of the vector $\tilde{\mathbf{q}}_n$ of generalized coordinates of the RFE *n*,

$$\tilde{\mathbf{q}}_n = \begin{bmatrix} \tilde{\mathbf{r}}_n \\ \tilde{\mathbf{\Phi}}_n \end{bmatrix}.$$

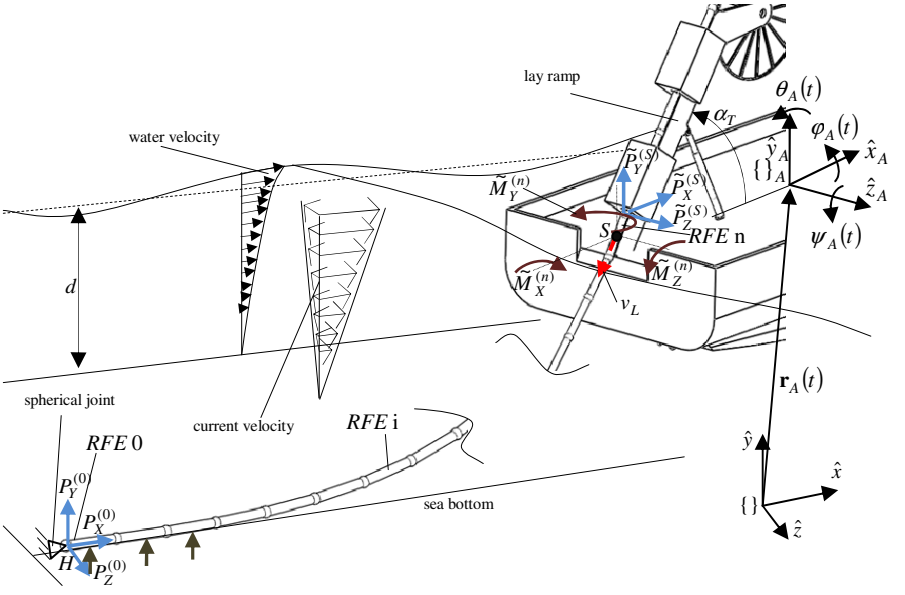

Fig. 9.27. Scheme of the system for installation of pipelines with the J-lay method

Differentiating (9.79) twice makes it possible to put the constraint equations in the accelerative form:

$$\begin{aligned} &\ddot{\tilde{\mathbf{r}}}_n + \ddot{\tilde{\mathbf{R}}}_n \tilde{\mathbf{r}}_s' + 2\dot{\tilde{\mathbf{R}}}_n \dot{\tilde{\mathbf{r}}}_s' + \tilde{\mathbf{R}}_n \ddot{\tilde{\mathbf{r}}}_s' = \mathbf{0}, \\ &\ddot{\tilde{\mathbf{\Phi}}}_n = \mathbf{0}. \end{aligned} \tag{9.80}$$

Since $\tilde{\mathbf{\Phi}}_n = \tilde{\mathbf{\Lambda}}_s = const$:

$$\begin{aligned} &\dot{\tilde{\mathbf{R}}}_n = \mathbf{0}, \\ &\ddot{\tilde{\mathbf{R}}}_n = \mathbf{0} \end{aligned} \tag{9.81}$$

so the equations (9.80) take the form:

$$\begin{aligned} &\ddot{\tilde{\mathbf{r}}}_n = -\tilde{\mathbf{R}}_n \ddot{\tilde{\mathbf{r}}}_s', \\ &\ddot{\tilde{\mathbf{\Phi}}}_n = \mathbf{0}. \end{aligned} \tag{9.82}$$

The equations of motion of the RFE n may be written as:

$$\begin{bmatrix} \tilde{\mathbf{m}}_n & \mathbf{0} \\ \mathbf{0} & \tilde{\mathbf{B}}_n \end{bmatrix} \begin{bmatrix} \ddot{\tilde{\mathbf{r}}}_n \\ \ddot{\tilde{\mathbf{\Phi}}}_n \end{bmatrix} - \begin{bmatrix} \tilde{\mathbf{P}}^{(n)} \\ \tilde{\mathbf{M}}^{(n)} \end{bmatrix} = \begin{bmatrix} \mathbf{Q}_n^{(\mathbf{r})} \\ \mathbf{Q}_n^{(\mathbf{\Phi})} \end{bmatrix}, \tag{9.83}$$

where $\mathbf{Q}_n^{(\mathbf{r})} = (\mathbf{Q}_n)_{i=1,2,3}$,

$\mathbf{Q}_n^{(\mathbf{\Phi})} = (\mathbf{Q}_n)_{i=4,5,6}$.

From (9.83) it follows:

$$\begin{aligned} \tilde{\mathbf{P}}^{(n)} &= \tilde{\mathbf{m}}_n \ddot{\tilde{\mathbf{r}}}_n - \mathbf{Q}_n^{(\mathbf{r})}, \\ \tilde{\mathbf{M}}^{(n)} &= \tilde{\mathbf{B}}_n \ddot{\tilde{\mathbf{\Phi}}}_n - \mathbf{Q}_n^{(\mathbf{\Phi})} = -\mathbf{Q}_n^{(\mathbf{\Phi})}. \end{aligned} \tag{9.84}$$

Components of the reaction $\tilde{\mathbf{P}}^{(n)}$ in the system of RFE n (which are needed e.g. to determine the tension) may be obtained from:

$$\tilde{\mathbf{P}}_n^{(n)} = \tilde{\mathbf{R}}_n^T \tilde{\mathbf{P}}^{(n)}. \tag{9.85}$$

The way of defining the vector $\tilde{\mathbf{r}}_s'$ giving the coordinates of the point S in the system $\{\}_n$ (Fig. 9.28) merits a further comment.

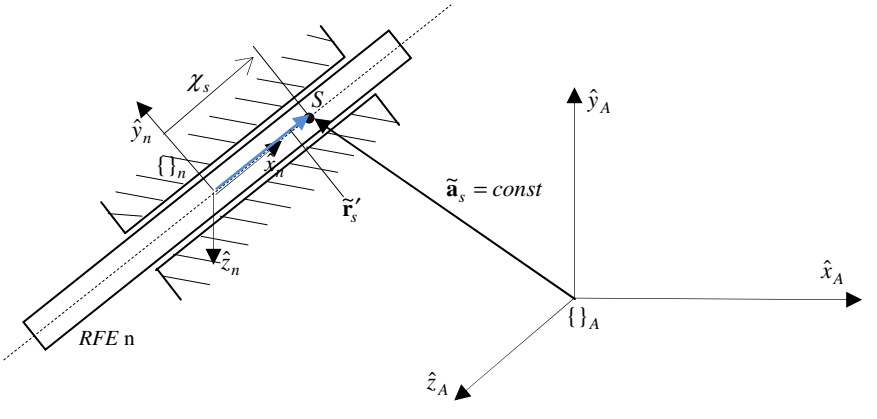

Fig. 9.28. Connection of the RFE n with the guide

In the situation of Fig. 9.28, the following holds:

$$\tilde{\mathbf{r}}_s' = \begin{bmatrix} \chi_s \\ 0 \\ 0 \end{bmatrix}, \tag{9.86}$$

where $\chi_s = \chi_s(t)$ is a function describing how the *n*-th *RFE* is ejected from the guide (velocity and possibly acceleration).

Static Analysis

Indirect verification was performed (by comparison with the calculations done employing the ANSYS package) on the J-lay system shown in Fig. 9.29. The total length of the analysed pipeline was 1000 m. Due to different positions of the initial point (*H*) of the pipeline attached with a joint to a rigid structure on the bottom the obtained curvatures of the pipeline and values of the forces and stresses differ. The models used are spatial, however, all the static forces act in the plane $\hat{x}\hat{y}$. Zero excitations were assumed ($\chi_s = const$, $\mathbf{q}_D = \mathbf{0}$, $H_S = 0$, no currents). The only forces acting on the pipeline were gravity and hydrostatic buoyancy. Data shown in Table 9.3 were assumed as input.

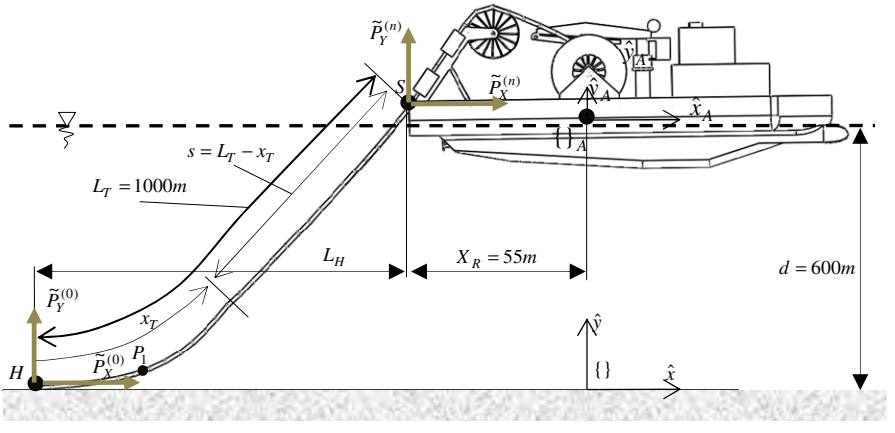

Fig. 9.29. Main parameters of a system in static analyses

Discretisation of the pipeline was performed for a few different numbers of finite elements (both for the programme *PipeLaySim* and the ANSYS package). Satisfactory correspondence was obtained already for the division into $n = 100$ elements (the results given below are for this number of elements). In ANSYS *PIPE288,* finite elements were used which are based on the *BEAM188* element

[Ansys Documentation, 2009] as well as linear shape functions. The element *PIPE288* supports input of hydrodynamic loads modelled using the commands: *OCDATA*, *OCTABLE*, *SOCEAN*. Results are shown on graphs and in tables using notation as in the following scheme (Fig. 9.30).

Table 9.3. Basic parameters assumed for static calculations

Parameter	Variant A	Variant B
Outer diameter of the pipeline [in]/side thickness [mm]	4/5.95	12/16.05
Content of the pipeline	Empty (air at atmospheric pressure) or filled (water under pressure equal to that outside)	
Distance L_H [m]	$L_H^{(1)}=700,\ L_H^{(2)}=725,\ L_H^{(3)}=750$	

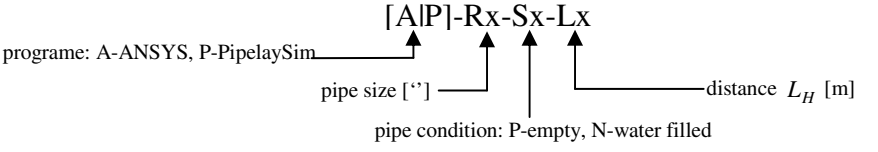

Fig. 9.30. Notation for cases of calculations

The analysis was performed with identical scenarios in both programmes. At the initial moment the pipeline was on the surface of water in undeformed state. In the first step, balance of the system was considered with gravity and buoyancy forces applied due to deflection and immersion of the pipeline's elements (with H being the loose end of the pipeline). Next, the point H of the pipeline was moved in multi-step static analysis to the destination point while keeping the point S motionless. Spherical joints were assumed in both points H and S. The results presented below correspond to the state of the system in the final step of computation. The reactions in the points H and S for a pipeline with diameter of 4 inches are shown in Table 9.4. Likewise, Table 9.5 contains the determined reactions of constraints for a pipeline with diameter of 12 inches.

Based on the performed comparative analyses a conclusion can be drawn that the results produced by the developed software are correct. The differences of forces calculated in the point S and of horizontal reactions in the point H are on average less than 0.5%. Also the values of the vertical reaction $\widetilde{P}_Y^{(0)}$ are in a satisfactory degree of accordance (the differences being 2–14% for pipes with diameters of 4 inches and 1–7% with diameters of 12 inches). The stated discrepancies are caused mainly by difficulties in modelling contact with the bottom which occur in the ANSYS environment.

Table 9.4. Reactions of constraints in points *H* and *S*, pipeline of 4 inches

Empty	[A|P]-R4-SP-L700	[A|P]-R4-SP-L725	[A|P]-R4-SP-L750
ANSYS	$\tilde{P}_X^{(n)} = 19.64$ $\tilde{P}_Y^{(n)} = 48.2$ $\tilde{P}_X^{(0)} = -19.79$ $\tilde{P}_Y^{(0)} = 0.54$	$\tilde{P}_X^{(n)} = 25.0$ $\tilde{P}_Y^{(n)} = 51.66$ $\tilde{P}_X^{(0)} = -25.1$ $\tilde{P}_Y^{(0)} = 0.53$	$\tilde{P}_X^{(n)} = 32.3$ $\tilde{P}_Y^{(n)} = 56.16$ $\tilde{P}_X^{(0)} = -32.4$ $\tilde{P}_Y^{(0)} = 2.18$
PipeLaySim	$\tilde{P}_X^{(n)} = 19.58$ $\tilde{P}_Y^{(n)} = 48.38$ $\tilde{P}_X^{(0)} = -19.58$ $\tilde{P}_Y^{(0)} = 0.49$	$\tilde{P}_X^{(n)} = 24.86$ $\tilde{P}_Y^{(n)} = 51.89$ $\tilde{P}_X^{(0)} = -24.86$ $\tilde{P}_Y^{(0)} = 0.49$	$\tilde{P}_X^{(n)} = 32.15$ $\tilde{P}_Y^{(n)} = 56.24$ $\tilde{P}_X^{(0)} = -32.15$ $\tilde{P}_Y^{(0)} = 2.23$
Filled	[A|P]-R4-SN-L700	[A|P]-R4-SN-L725	[A|P]-R4-SN-L750
ANSYS	$\tilde{P}_X^{(n)} = 49.07$ $\tilde{P}_Y^{(n)} = 121.6$ $\tilde{P}_X^{(0)} = -49$ $\tilde{P}_Y^{(0)} = 0.31$	$\tilde{P}_X^{(n)} = 62.55$ $\tilde{P}_Y^{(n)} = 129.4$ $\tilde{P}_X^{(0)} = -62.5$ $\tilde{P}_Y^{(0)} = 0.48$	$\tilde{P}_X^{(n)} = 80.89$ $\tilde{P}_Y^{(n)} = 140.6$ $\tilde{P}_X^{(0)} = -80.8$ $\tilde{P}_Y^{(0)} = -6.23$
PipeLaySim	$\tilde{P}_X^{(n)} = 48.99$ $\tilde{P}_Y^{(n)} = 122.06$ $\tilde{P}_X^{(0)} = -48.99$ $\tilde{P}_Y^{(0)} = 0.27$	$\tilde{P}_X^{(n)} = 62.49$ $\tilde{P}_Y^{(n)} = 130.0$ $\tilde{P}_X^{(0)} = -62.49$ $\tilde{P}_Y^{(0)} = 0.46$	$\tilde{P}_X^{(n)} = 80.78$ $\tilde{P}_Y^{(n)} = 141.2$ $\tilde{P}_X^{(0)} = -80.78$ $\tilde{P}_Y^{(0)} = -6.42$

The shape of the pipeline in the $\hat{x}\ \hat{y}$ plane is shown in Fig. 9.31. The presented results are for the empty pipeline with a diameter of 4 inches. Differences in the values are small and do not exceed 0.1%. Similar results were obtained for the pipeline with a diameter of 12 inches.

The influence of the pipeline's shape on the reduced stresses for the considered cases is presented in Fig. 9.32 (for a pipeline with diameter of 4 inches) and Fig. 9.33 (for a pipeline with diameter of 12 inches). In the analyses, the Huber-Mises-Hencky (HMH) hypothesis was assumed for the calculation of reduced stresses. The graphs show bending moments, axial forces and reduced stresses in sections along the relative length defined by the coordinate $\gamma = \frac{x_T}{L_T}$ ($\gamma = 0$ in

Table 9.5. Reactions of constraints in points *H* and *S*, pipeline of 12 inches

Empty	[A|P]-R12-SP-L700	[A|P]-R12-SP-L725	[A|P]-R12-SP-L750
ANSYS	$\tilde{P}_X^{(n)} = 130$ $\tilde{P}_Y^{(n)} = 319.3$ $\tilde{P}_X^{(0)} = -131$ $\tilde{P}_Y^{(0)} = 3.72$	$\tilde{P}_X^{(n)} = 165.7$ $\tilde{P}_Y^{(n)} = 342.2$ $\tilde{P}_X^{(0)} = -166.1$ $\tilde{P}_Y^{(0)} = 2.65$	$\tilde{P}_X^{(n)} = 214.1$ $\tilde{P}_Y^{(n)} = 371.4$ $\tilde{P}_X^{(0)} = -214.2$ $\tilde{P}_Y^{(0)} = -14.28$
PipeLay Sim	$\tilde{P}_X^{(n)} = 128.7$ $\tilde{P}_Y^{(n)} = 320.0$ $\tilde{P}_X^{(0)} = -128.7$ $\tilde{P}_Y^{(0)} = 3.58$	$\tilde{P}_X^{(n)} = 165.1$ $\tilde{P}_Y^{(n)} = 343.1$ $\tilde{P}_X^{(0)} = -165.1$ $\tilde{P}_Y^{(0)} = 2.48$	$\tilde{P}_X^{(n)} = 213.8$ $\tilde{P}_Y^{(n)} = 371.5$ $\tilde{P}_X^{(0)} = -213.8$ $\tilde{P}_Y^{(0)} = -15.1$
Filled	[A|P]-R12-SN-L700	[A|P]-R12-SN-L725	[A|P]-R12-SN-L750
ANSYS	$\tilde{P}_X^{(n)} = 394$ $\tilde{P}_Y^{(n)} = 969.9$ $\tilde{P}_X^{(0)} = -393.5$ $\tilde{P}_Y^{(0)} = 5.55$	$\tilde{P}_X^{(n)} = 502.3$ $\tilde{P}_Y^{(n)} = 1038.1$ $\tilde{P}_X^{(0)} = -501.8$ $\tilde{P}_Y^{(0)} = 5.9$	$\tilde{P}_X^{(n)} = 649.15$ $\tilde{P}_Y^{(n)} = 1129.3$ $\tilde{P}_X^{(0)} = -648.9$ $\tilde{P}_Y^{(0)} = -41.6$
PipeLay Sim	$\tilde{P}_X^{(n)} = 393.4$ $\tilde{P}_Y^{(n)} = 967.87$ $\tilde{P}_X^{(0)} = -393.4$ $\tilde{P}_Y^{(0)} = 5.88$	$\tilde{P}_X^{(n)} = 501.7$ $\tilde{P}_Y^{(n)} = 1040.2$ $\tilde{P}_X^{(0)} = -501.7$ $\tilde{P}_Y^{(0)} = 6.01$	$\tilde{P}_X^{(n)} = 648.78$ $\tilde{P}_Y^{(n)} = 1032.1$ $\tilde{P}_X^{(0)} = -648.78$ $\tilde{P}_Y^{(0)} = -41.9$

the point H and $\gamma = 1$ for the point *S*, Fig. 9.29). As it can be seen from the graphs, the RFE method gives close results also for reduced stresses, bending forces and moments in sections of the pipeline. Relative errors in all cases are below 1–1.5% (for the given number of elements) and definitely diminish with condensation of the division.

Analysing the graphs in Fig. 9.32 and Fig. 9.33 indicates that filling the pipeline with a liquid does not influence the forms of the bending moment (in the considered cases similar curvatures were obtained for an empty and filled pipeline). The axial force, which depends on the position of the vessel against the waves and density of the pipeline, has significant influence on the values of reduced stresses. Installation of pipelines when they are filled with air allows for reducing the axial forces and stresses.

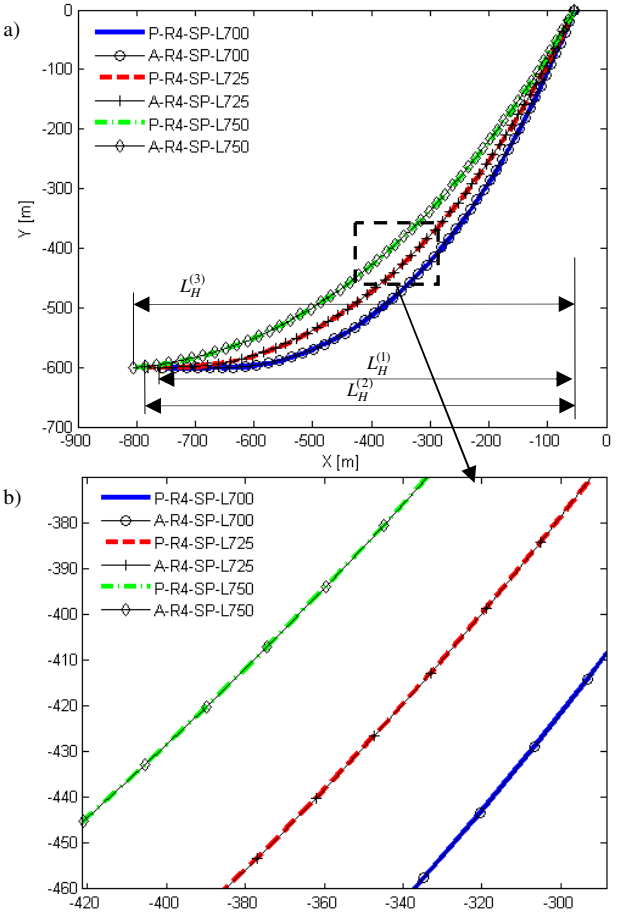

Fig. 9.31. Shape of a pipeline with diameter of 4 inches having reached static balance: a) shape of the pipeline obtained for different values of L_H , b) magnified fragment of the graph

The described method of static analysis and the obtained results may inform the determination of installation parameters of the pipeline concerned, taking into consideration the influence of depth, buoyancy and geometric traits of the system [Mohitpour M., et al., 2003], [Bai Y., Bai Q., 2005], [Palmer A. C., King R. A., 2008].

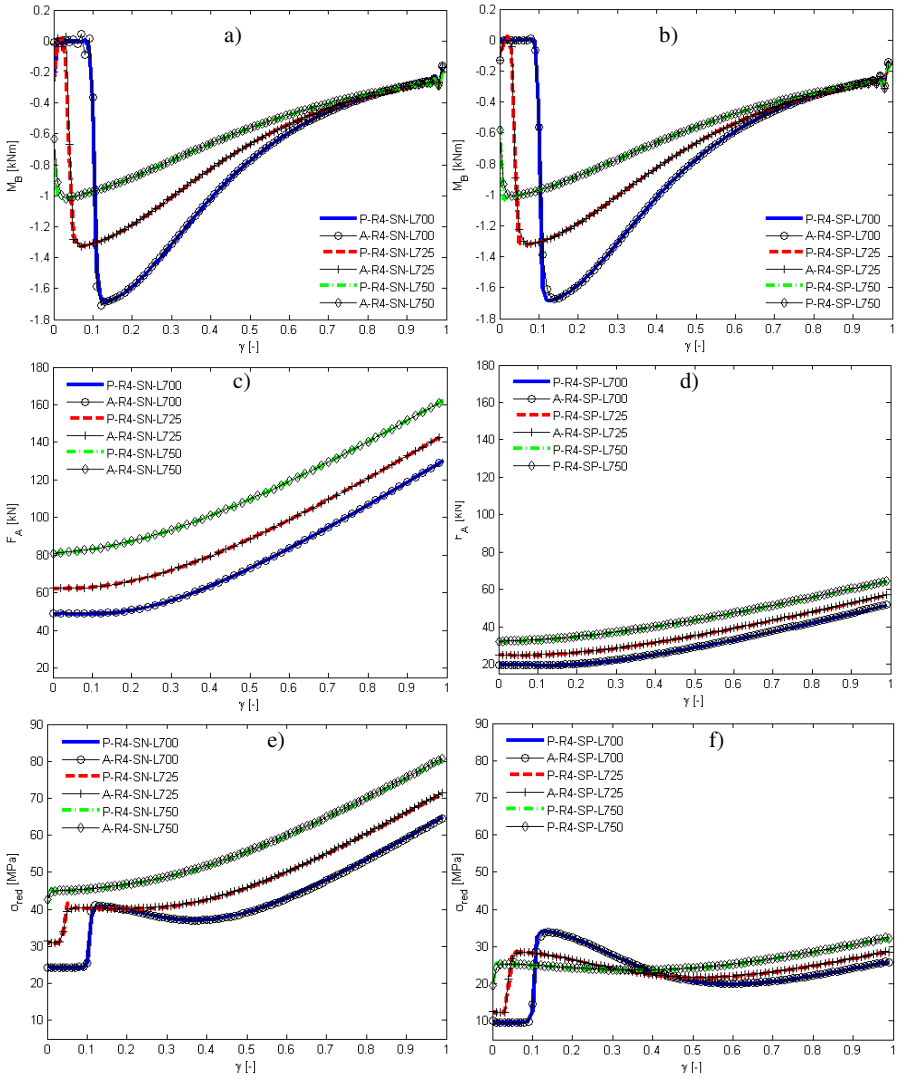

Fig. 9.32. A pipeline with diameter of 4 inches – values of moments, forces and stresses: bending moment for a filled (a) and empty (b) pipeline, axial force in a section of a filled (c) and empty (d) pipeline, reduced stress for a filled (e) and empty (f) pipeline

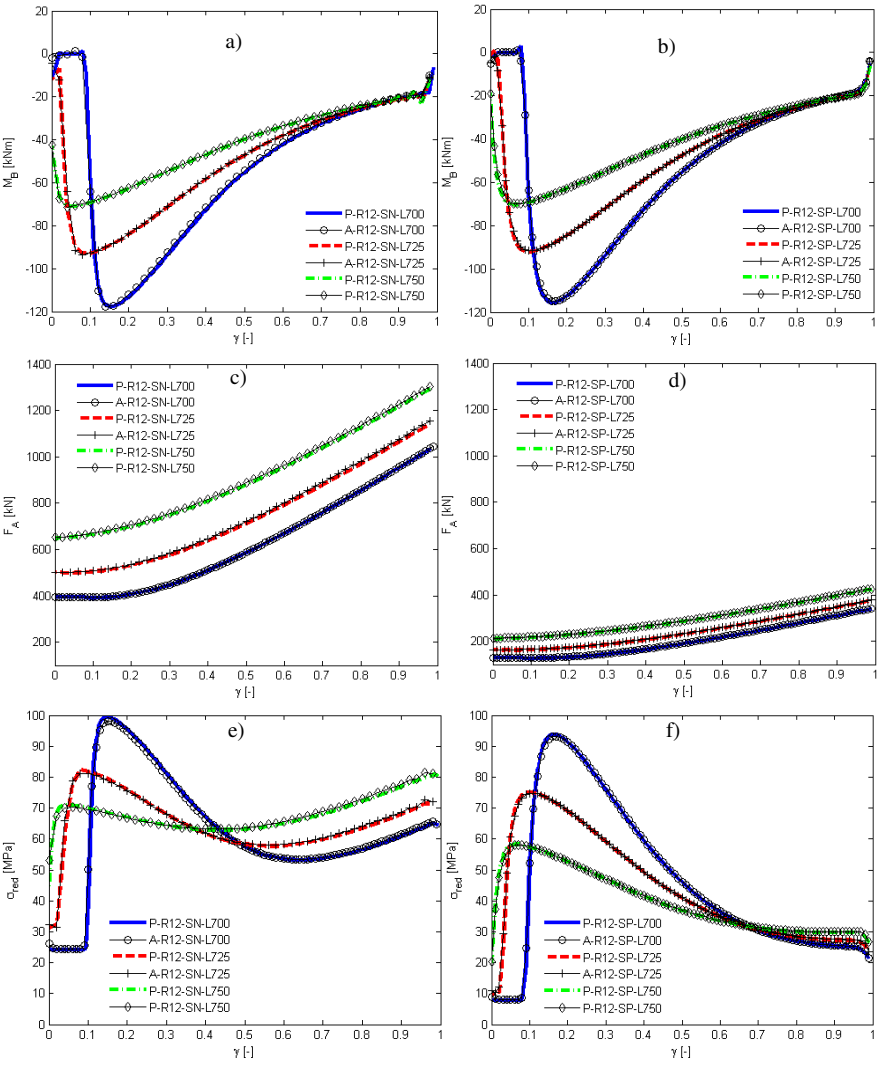

Fig. 9.33. A pipeline with diameter of 12 inches – values of moments, forces and stresses: bending moment for a filled (a) and empty (b) pipeline, axial force in a section of a filled (c) and empty (d) pipeline, reduced stress for a filled (e) and empty (f) pipeline

Dynamic Analysis

This part of the book contains a brief overview of the results of analyses pertaining to the dynamics of the analysed system. Again, the programmes *PipeLaySim* and ANSYS were used and the obtained results compared. The same geometry and mass parameters were assumed as for the static analyses. As the initial conditions in the dynamic problem (at time $t = 0$) the values yielded by the last step of the static analysis were taken. The fourth-order Runge-Kutta method with constant integration step was used in the *PipeLaySim* programme to integrate the equations of motion [Press W. H., 2002], whereas in the ANSYS package the Newmark method [Bathe K. J., 1996] was used.

Two types of excitation were applied. In the first case (W1), no waves $(H_S = 0\,\mathrm{m})$ was assumed and a harmonic excitation of the vessel's immersive motion (Fig. 9.34a) with amplitudes and periods listed in Table 9.6. This case corresponds to motion of the system immersed in a motionless liquid. The second type of excitation (W2) included both the motion of the vessel and waves of the water (calculations in both programmes were performed according to the Airy model of the wave). Graphs of the excitations are shown in Fig. 9.34b, assuming appropriate resizing of amplitudes in the initial phase of calculations and a phase shift for the variable x_D equal $\varphi_X^{(0)} = 90°$. The lower rows of Table 9.6 contain the remaining parameters, which are common to the cases W1 and W2. $\chi_s = const$ was assumed in both programmes.

Table 9.6. Parameters assumed in the dynamic analysis

Excitation	H_S [m]	A_X [m], $\varphi_X^{(0)}$ [deg]	A_Y [m], $\varphi_Y^{(0)}$ [deg]	Period T [s]
W1	0.0	0; 0	1; 0	8.0
W2	5.0	1; 90	2; 0	8.0
Coeff. C_D / C_A from (3.33)		1.0/1.0	Stiffness coeff. of the seabed	1.1e^5 N/m
Data set (geometry, diameter, content of the pipeline)		R4-SP-L700	Tangent resistance coefficients m and n (Table 3.3)	$m = 0.02$ $n = 0.04$

Fig. 9.35 presents time courses of coordinates of the point P_1 of the pipeline at the maximum of curvature (Fig. 9.29) determined by the coordinate $x_T = 250$ m. In both cases of the vessel's motion and waves, the graphs of displacements of the point are similar. Relative errors do not exceed 1%.

In Fig. 9.36, the velocities P_1 obtained from both programmes are presented. The produced graphs are virtually identical. The differences are due to integration methods and also to the accuracy with which the excitation is realized. In ANSYS,

it was interpolated with a piecewise linear function (boundary conditions for the displacements given as tables).

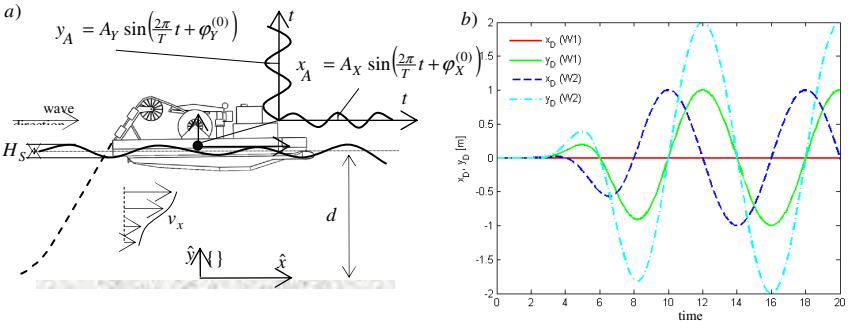

Fig. 9.34. Excitations of the vessel's motion in dynamic analysis: a) assumed conditions of waves and vessel's motion, b) graphs of longitudinal rolling x_A and heave y_A

Dynamic reactions at the point S (the point of connection with the guiding device onboard the vessel) are shown in Fig. 9.37. In the case of vertical reaction $R_Y^{(S)}$ the maximal relative error does not exceed 10% (W2 excitation).

The reduced stresses calculated along the pipeline's axis are shown in Fig. 9.38. The graphs were produced for the time $t = 10$ s taking dynamic forces into account.

On the comparative results of static and dynamic analyses presented a conclusion can be based that the proposed model and software are correct. Since actual objects (ships for laying pipelines) are hardly available and laboratory research is very costly and requires large pools and devices producing artificial waves, performing empirical tests is rather difficult. The authors are aware that results of measurements obtained from tests on actual objects may deviate from the values yielded by the process of numerical simulation, among other things due to the simplified description of interaction in the liquid – solid body system and the approximate model of waves. Yet, some verification is assured by comparing the results with that from another environment aimed at modelling and analyses (e.g. of the ANSYS type) which is commonly used and has been verified multiple times. This allows us to eliminate some possible errors in modelling and programming.

9.3.2 Installation of a Pipeline with the S-Lay Method

A mathematical model of a system for simulating the dynamics of the installation process with the S-lay method can be formulated by augmenting the model of the

J-lay method. The additional element is a specialized ramp guiding the pipeline (a *stinger*) (Fig. 9.39). In the model presented herein, the ramp is assumed to be a bent beam with variable section modelled with the classical finite element method connected by a joint to the vessel's deck at the point U and additionally with two supporting ropes.

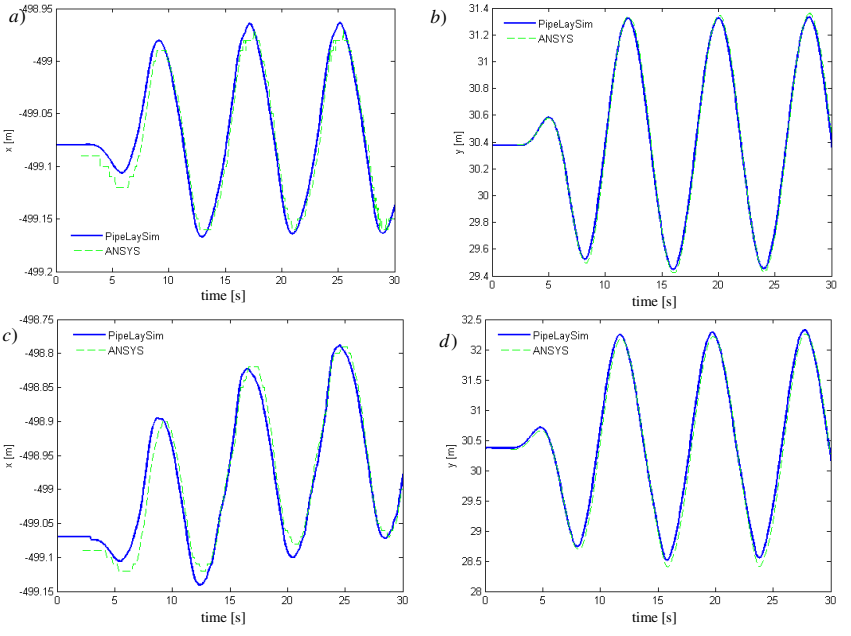

Fig. 9.35. Coordinates of the point xx of the pipeline: a) coordinate x (W1), b) coordinate y (W1), c) graph of the coordinate x (W2), d) graph of the coordinate y (W2)

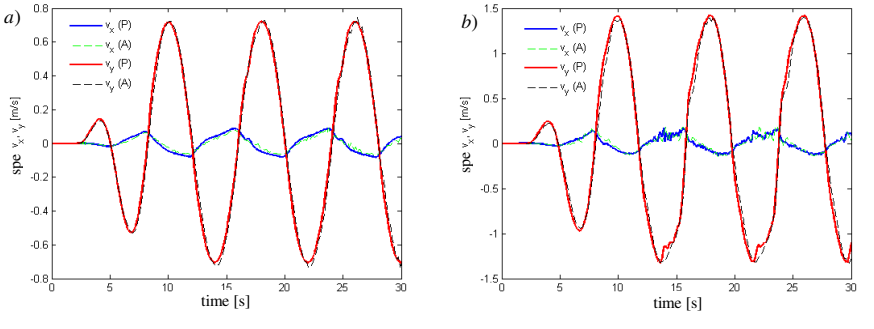

Fig. 9.36. Velocities of the point P_1 : a) W1 excitation, b) W2 excitation

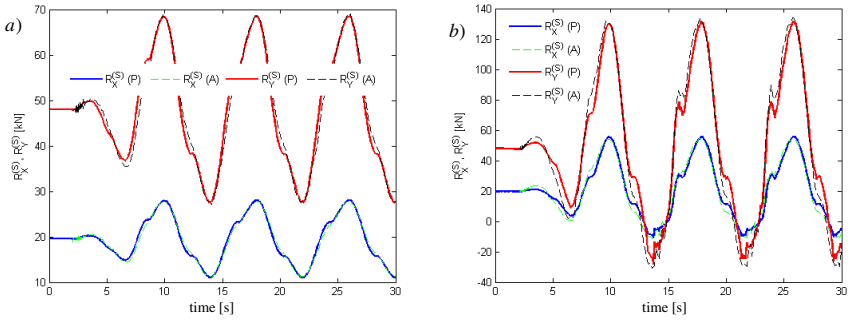

Fig. 9.37. Dynamic reactions at the point *S*: a) W1 excitation, b) W2 excitation

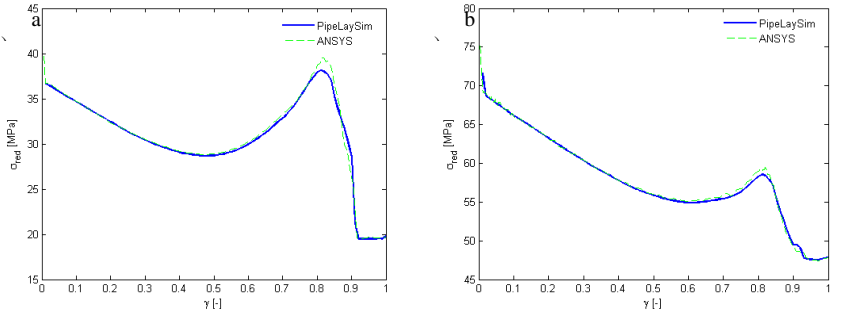

Fig. 9.38. Reduced stresses for the time *t*=10s: a) W1 excitation, b) W2 excitation

The model of the pipeline is similar to that used for the J-lay method. It is described in the previous chapter. A model of the ramp connected with the deck by a joint *U* and supporting ropes needs to be additionally formulated. Hence, the equations of motion of the system may be written in the form [Szczotka M., 2011b]:

$$\mathbf{A}^{(J)}\ddot{\tilde{\mathbf{q}}}^{(J)} = \mathbf{Q}^{(J)} + \mathbf{Q}^{(J,C)}, \tag{9.87}$$

$$\mathbf{A}^{(R)}\ddot{\tilde{\mathbf{q}}}^{(R)} = \mathbf{Q}^{(R)} + \mathbf{Q}^{(R,C)} + \mathbf{Q}^{(R,L)}, \tag{9.88}$$

where $\mathbf{A}^{(J)}$ – matrix of masses of the pipeline,

$\tilde{\mathbf{q}}^{(J)} = \begin{bmatrix} \tilde{\mathbf{q}}_0^{(J)} \\ \vdots \\ \tilde{\mathbf{q}}_n^{(J)} \end{bmatrix}$ – vector of generalized coordinates of the pipeline,

$\mathbf{Q}^{(J)}$ – vector of generalized forces acting on the pipeline,

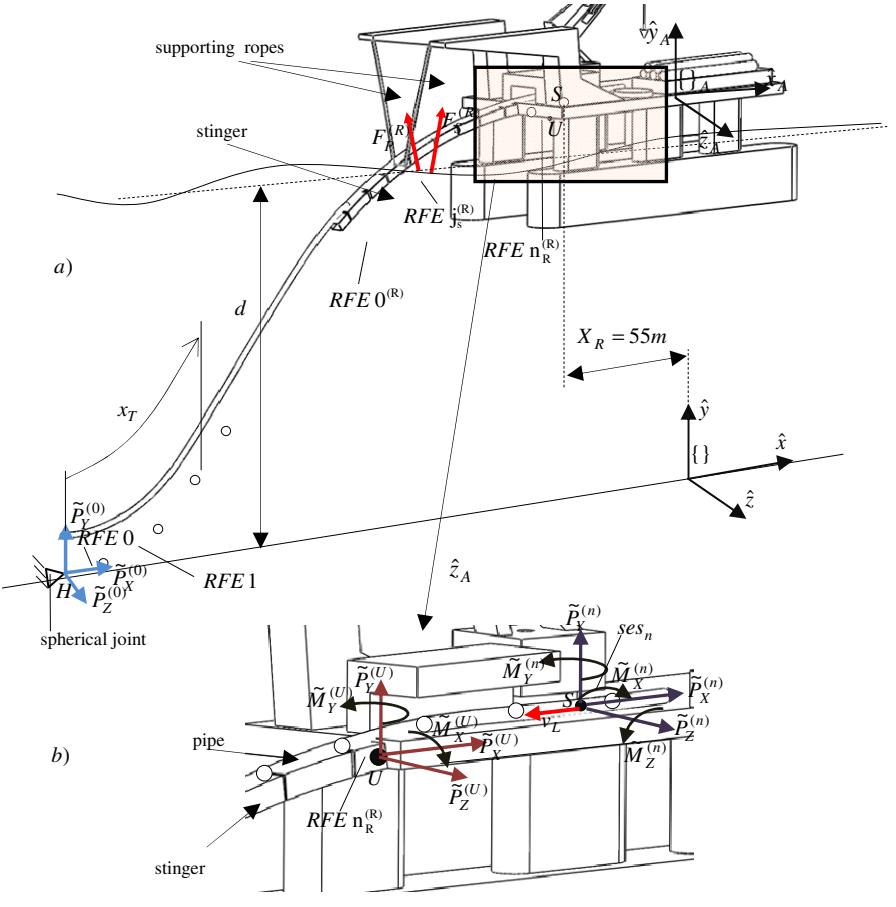

Fig. 9.39. Scheme of the model for the analysis of installing a pipeline with the S-lay method: a) positioning of the coordinate systems, b) reactions of constraints

$\mathbf{Q}^{(J,C)}$ – vector of generalized forces exerted by the ramp,

$\mathbf{A}^{(R)}$ – matrix of masses of the ramp,

$\tilde{\mathbf{q}}^{(R)} = \begin{bmatrix} \tilde{\mathbf{q}}_0^{(R)} \\ \vdots \\ \tilde{\mathbf{q}}_{n_R}^{(R)} \end{bmatrix}$ – vector of generalized coordinates of the ramp,

$\mathbf{Q}^{(R)}$ – vector of generalized forces acting on the ramp,

$\mathbf{Q}^{(R,C)}$ – vector of generalized forces exerted by the pipeline,

$\mathbf{Q}^{(R,L)}$ – vector of generalized forces due to the actions of forces supporting the structure of the ramp.

The equations and reactions of constraints imposed on the pipeline are identical to those of the J-lay model. Whereas the joint at the connection of the ramp with the deck (a revolute connection) makes it necessary to include the reaction vector:

$$\tilde{\mathbf{P}}^{(U)} = \left[\tilde{P}_X^{(U)} \quad \tilde{P}_Y^{(U)} \quad \tilde{P}_Z^{(U)}\right]^T, \tag{9.89}$$

and a vector of the pair of forces whose moment is:

$$\tilde{\mathbf{M}}^{(U)} = \left[\tilde{M}_X^{(U)} \quad \tilde{M}_Y^{(U)}\right]^T. \tag{9.90}$$

By neglecting friction in the connection, $\tilde{M}_Z^{(U)} = 0$ is assumed.

The constraint equations take the form:

$$\tilde{\mathbf{r}}^{(U)} = \tilde{\mathbf{r}}_{n_R}^{(R)} + \tilde{\mathbf{R}}_{n_R}^{(R)} \tilde{\mathbf{r}}_{n_R}^{\prime(U)} = const, \tag{9.91}$$

$$\mathbf{\Lambda}_2 \tilde{\mathbf{\Phi}}_{n_R}^{(R)} = const, \tag{9.92}$$

where $\tilde{\mathbf{r}}_{n_R}^{\prime(U)}$ – vector of generalized coordinates of the point U in the system of the RFE n_R of the ramp,

$\tilde{\mathbf{r}}_{n_R}^{(R)}, \tilde{\mathbf{\Phi}}_{n_R}^{(R)}$ – vectors of components of the vector $\tilde{\mathbf{q}}_{n_R}^{(R)} = \begin{bmatrix} \tilde{\mathbf{r}}_{n_R}^{(R)} \\ \tilde{\mathbf{\Phi}}_{n_R}^{(R)} \end{bmatrix}$,

$\tilde{\mathbf{R}}_{n_R}^{(R)}$ – rotation matrix of the n_R of the ramp,

$\mathbf{\Lambda}_2 = \begin{bmatrix} 1 & 0 & 0 \\ 0 & 1 & 0 \end{bmatrix}$.

Following the procedure presented in the previous chapter the constraint equations may be put in an accelerative form allowing us to determine the vectors $\tilde{\mathbf{P}}^{(U)}$, $\tilde{\mathbf{M}}^{(U)}$ and $\ddot{\tilde{\mathbf{q}}}_{n_R}^{(R)}$. Actions of the following forces are also taken into account:

- in the ropes $F_S^{(R)}$, $F_P^{(R)}$ acting on $\mathrm{REF}_{j_s}^{(R)}$ introduced by the vector $\mathbf{Q}^{(R,L)}$,
- contact forces, acting on elements of the pipeline and on the ramp, derived from $\mathbf{Q}^{(J,C)}$ and $\mathbf{Q}^{(R,C)}$.

Forces in the ropes may be determined using the model of a flexible rope with damping. The contact forces between the ramp and the pipeline are determined by assuming a series of spring-damping elements with clearance modelling the rollers guiding the pipeline. The forces of interaction of the ramp's structure with the water environment are approximated with the Morison equation keeping in mind the additional interactions occurring at the transition through the water surface.

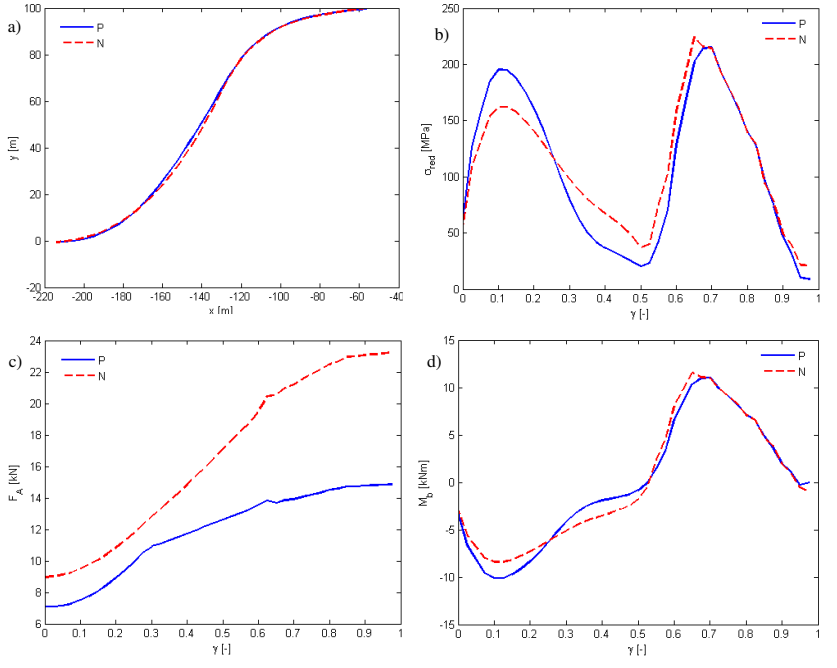

Fig. 9.40. Results obtained from static analysis of the S-lay system: a) shape of the pipeline, b) reduced stresses, c) graph of the axial force, d) bending moment

Sample calculations contained in this section were performed for an installation of a pipeline of 4 inches at the depth of $d = 100$ m. The shape of the pipeline after it has reached static balance is shown in Fig. 9.40a, where the coordinates on the graph are expressed in the inertial system $\{\}$ depicted in Fig. 9.39a. Two options were considered: on the graphs P denotes a pipeline filled with air, N – a pipeline filled with water. Graphs of reduced stresses along the pipeline's axis (Fig. 9.40b) are different to those obtained in the J-lay method. Two places occur with considerable stresses due to bending. The first one is caused by the ramp's curvature (a section called *overbend*), the second results from the curvature of the pipeline above the bottom (*sagbend*).

Stresses in the pipeline may be controlled by changing: the immersion of the ramp, its shape and the value of the force stretching the pipeline. The bending moment being zero at some point (Fig. 9.40d) is also characteristic of this method.

Sample results of calculations of the dynamics are shown in Fig. 9.41. Harmonic motion of the vessel with period $T = 8\,\mathrm{s}$ and amplitudes $x_A = 0.5\,\mathrm{m}$, $y_A = 1.0\,\mathrm{m}$ was taken as the excitation. The coefficients of the Morison equation were assumed as in previous analyses.

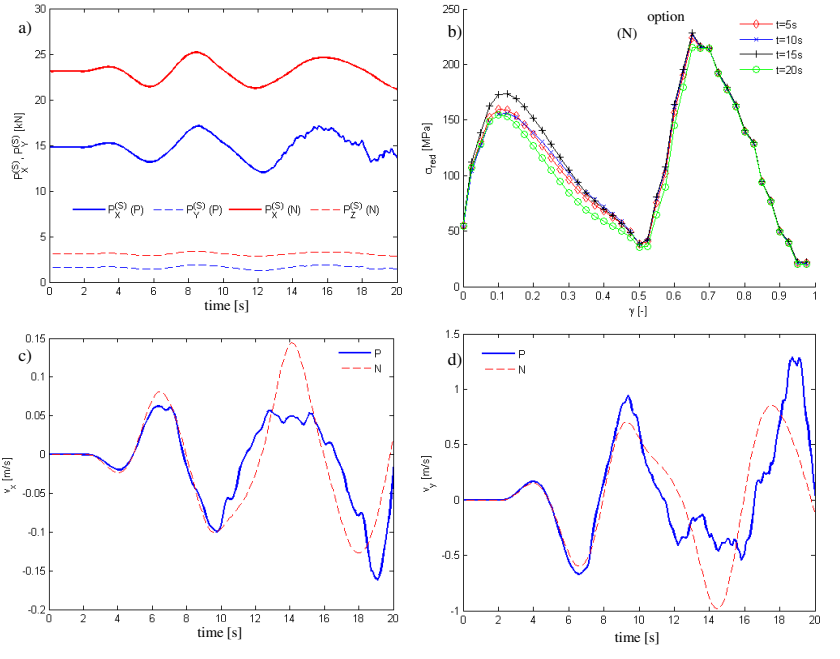

Fig. 9.41. Simulation of the dynamics of a system for S-lay installation: a) dynamic reactions at the point *S*, b) reduced stresses in selected points of time, c) graphs of the horizontal component of velocity in time, d) graphs of the vertical component of velocity in time

The dynamic reactions at the point *S* (Fig. 9.41a) (guiding the RFE *n* in the tensioner's mechanism) are not significantly different from the values obtained in the static problem due to the assumed length and size of the pipeline (the mass is fairly small). Additionally, as Fig. 9.41b implies, in which graphs of the reduced stresses at different points in time are presented, with a relatively rigid system of ramps the change of values of the stresses occurs in the lower segment of the pipeline only. The changes would be greater with a more flexible ramp (or suspension system), which may result, when the length of the system is significant, in considerable differences in the geometry of the lower segment of the pipeline (*sagbend*). A possibility also exists of controlling the lengths of the ropes in such a way that the growth of stresses caused by waves is eliminated. The velocities of the centre of mass of the RFE located approximately 4 m above the

bottom of the sea are shown on graphs (Fig. 9.41 c and d). In the case of the S-lay method, the differences in the velocities of the pipeline in the lower part are greater for different contents of the pipeline (densities) than with the J-lay method.

9.3.3 Dynamics of a System for Installing Pipelines with the Reel Method

Dependencies presented in the preceding chapters allow us to formulate mathematical models and a computer programme suitable for simulating the operation of a device for laying pipelines with the reel method. The section presents a model for the analysis of the dynamics of a system equipped with a passive reel drive system. To discretize the pipeline the modified RFE method is used and the nonlinear dependency of stresses on deformations is described by an elasto-plastic characteristic. Models contained herein are investigated in [Szczotka M., 2010], [Szczotka M., 2011b].

9.3.3.1 Mathematical Model

In Fig. 9.42, a scheme is shown of a system consisting of a reel onto which the pipeline is wound and a specialized guiding ramp through which the pipe passes as it is unwound and lowered to the seabed. The ramp is equipped with devices controlling the tension and the speed of laying.

The following simplifying assumptions are made:

- the motion of the pipeline being unwound from the reel is kinematically forced by a device providing tension and guidance; influence of the immersed part of the pipeline on the motion may be neglected,
- swaying angle ψ_A of the vessel is the most important parameter of the lifting motion, therefore a simplification is proposed which reduces the problem to a planar system in which the vessel can move according to the known functions:

$$\begin{aligned} x_A &= \Im\left(t, \mathbf{RAO}, H_S, T_Z, \beta_f, S(\omega)\right), \\ y_A &= \Im\left(t, \mathbf{RAO}, H_S, T_Z, \beta_f, S(\omega)\right), \\ \psi_A &= \Im\left(t, \mathbf{RAO}, H_S, T_Z, \beta_f, S(\omega)\right), \\ z_A(t) &= 0, \quad \theta_A(t) = 0, \quad \varphi_A(t) = 0, \end{aligned} \tag{9.93}$$

where $\Im$ – operator of transformation of the motion from the domain of frequency to the domain of time,

H_S, T_Z – height and period of waves,

β_f – wave's angle of attack,

$S(\omega)$ – defined by (3.27) or (3.28),

RAO – operator of the transition function,

- large deflections of the pipeline are taken into account by applying the modified RFE method including bending in the longitudinal plane of the vessel.

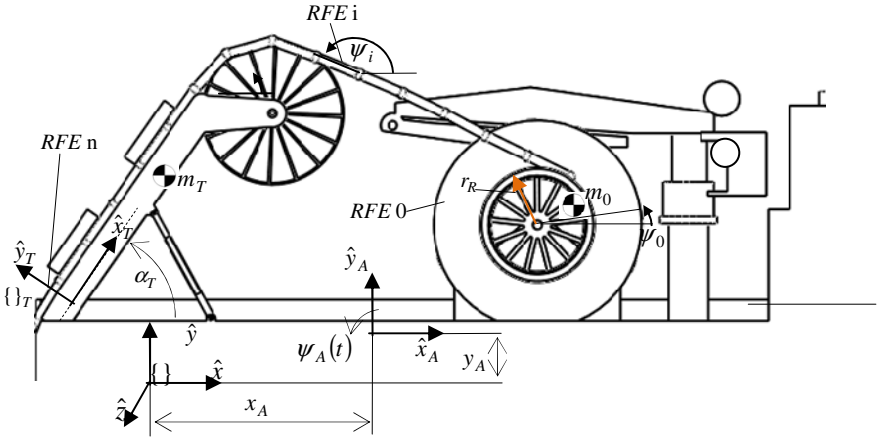

Fig. 9.42. Scheme of the reel system

The generalized coordinates of the considered system are therefore components of the following vector **q**, (an appropriate choice of mass, inertia and geometric parameters allows the reel to be treated as RFE 0):

$$\mathbf{q} = [\psi_0, ..., \psi_i, ..., \psi_n, \alpha_T]^T, \tag{9.94}$$

where ψ_i – inclination of the axes of the RFE *i* to the axes $\hat{x}_B$ of the inertial system,

α_T – inclination angle of the ramp's axis.

The equations of motion along with the constraint equations may be written as (detailed derivations are presented in the papers [Szczotka M., 2010], [Szczotka M., 2011b]):

$$\begin{aligned} \mathbf{A}\ddot{\mathbf{q}} + \mathbf{B}\dot{\mathbf{q}} - \mathbf{DP} &= \mathbf{Q} - \mathbf{G} - \mathbf{H}, \\ -\mathbf{S}\ddot{\mathbf{q}} &= \mathbf{W}, \end{aligned} \tag{9.95}$$

where $\mathbf{A} = \mathbf{A}(t, \mathbf{q})$ – matrix of inertia of the system,

$\mathbf{B} = \mathbf{B}(t, \mathbf{q}, \dot{\mathbf{q}})$,

$\mathbf{D}(\mathbf{q}), \mathbf{S}(\mathbf{q})$ – matrices of coefficients of reactions and constraint equations,

$\mathbf{Q}(t,\mathbf{q},\dot{\mathbf{q}})$ – vector of generalized forces,

$\mathbf{G}$ – vector taking the potential of gravity forces into account,

$\mathbf{H}=\mathbf{H}(t)$ – vector whose components depend on the base's lifting motion,

$\mathbf{W}(t,\mathbf{q},\dot{\mathbf{q}})$ – vector of the right-hand sides of the constraint equation,

$\mathbf{P}$ – vector of unknown reactions of the constraints.

The equations (9.95) were integrated with the fourth-order Runge-Kutta method with a constant step of integration. Determination of the initial conditions for the system's equations of motion requires solving sequentially a few static and quasi-static problems. If in the equations (9.95) the following is assumed:

$$\ddot{\mathbf{q}}=\dot{\mathbf{q}}=\mathbf{0}, \tag{9.96}$$

then the static problem requires solving a system of nonlinear algebraic equations of the form:

$$\begin{aligned}\boldsymbol{\Psi}(\mathbf{q}_s)&=\mathbf{0},\\ \boldsymbol{\Phi}(\mathbf{R}_s)&=\mathbf{0},\end{aligned} \tag{9.97}$$

where $\boldsymbol{\Psi}(\mathbf{q})=\mathbf{0}$ – equations of balance of the RFEs 1,...,*n* and the guiding ramp,

$\mathbf{q}_s=[\psi_1,...,\psi_n,\psi_T]^T$,

$\mathbf{R}_s=[U_E,N_E,M_n]^T$,

$\boldsymbol{\Theta}(\mathbf{R}_s)=\mathbf{0}$ – constraint equations.

Solving the system of equations (9.97) was done with the Newton method. The procedure preceding the calculations of the dynamics is depicted in Fig. 9.43. In the first stage, the pipeline is wound onto the reel. At this time plastic deformations may occur. The end of the pipe is transferred to the guiding ramp in the next stage. Having performed these calculations, we obtain the initial conditions assumed as the starting point of the dynamics.

In the computer programme, a possibility is also included to perform dynamic analysis with a simplified model in which oscillations (dynamics) are not included (the model is introduced in [Szczotka M., et al., 2007). In such case, an internal procedure solving the equations (9.97) with the Newton method determines the forces occurring during the unwinding of the pipeline when integrating the reel's equations of motion. The equation of the reel's dynamics may be obtained from the equations (9.95) assuming $n=0$ and taking into account the forces caused by deformations of the pipeline described by the system of equations (9.97). Note, however, that despite the minimal dimension of the model, the necessity of using the Newton method, which is sensitive to nonlinearity of the problem considered,

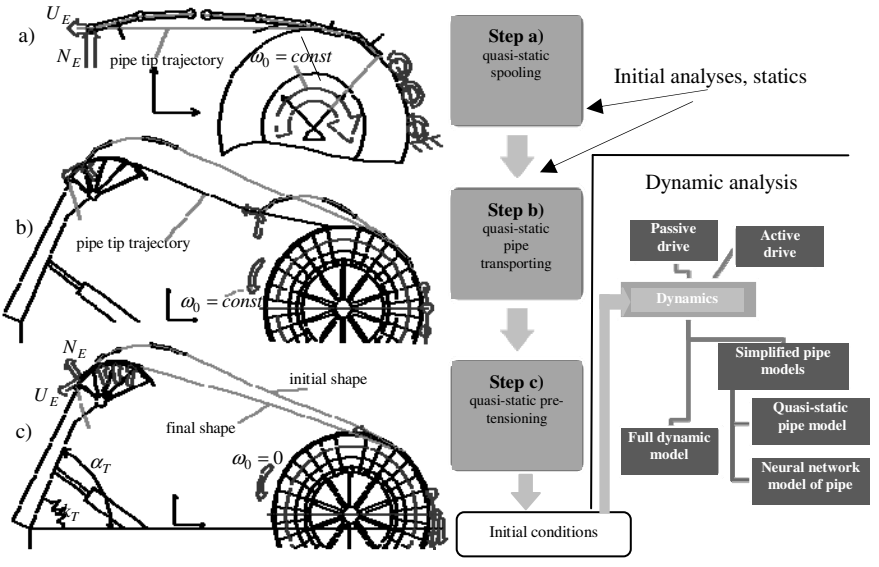

Fig. 9.43. Quasi-static analyses for determining the initial conditions: a) stage of winding the pipe onto the reel, b) transferring the pipe to the ramp, c) stretching the system to the nominal tension

lengthens the durations of computer simulations with respect to the full model of the dynamics. Those durations are approximately ten times longer, therefore using this model does not seem prudent. Hence, another approach to employing the simplified model is proposed. The discrete model of the pipeline is thereby replaced with an artificial neural network [Szczotka M., 2010]. Minimal computation time is then required to determine the forces due to the pipeline's work as it is being unwound, and use them in the equation of the reel's dynamics. Computational efficiency of a such model is particularly appealing. It also lends itself somewhat to real-time control. The results obtained from both variants of the model are presented later in this chapter.

9.3.3.2 Calculations for a Passive Drive of the Reel

The results of calculations performed for the system shown in Fig. 9.42 are presented below. The drive of the reel from which the pipeline is unwound is assumed to be passive and to exert a constant force applied at a dividing radius of the clockwork. To make the interpretation of the results more convenient, the simulations were performed assuming the following functions describing the motion of the vessel:

$$\begin{aligned} x_A &= A_X \sin(\omega t + \gamma_X), \\ y_A &= A_Y \sin(\omega t + \gamma_Y), \\ \psi_A &= A_\psi \sin(\omega t + \gamma_\psi), \end{aligned} \tag{9.98}$$

where A_X, A_Y, A_ψ – amplitudes of motion in the appropriate directions,

$\gamma_X, \gamma_Y, \gamma_\psi$ – initial phases,

ω – angular frequency of excitation.

Basic assumed parameters of the device are based on the documentation of one of the devices operating on the North Sea. The characteristic values are gathered in Table 9.7 (the dimensions and parameters are shown in Fig. 9.42). The objective of the performed simulations was to determine the influence of waves and braking force of the reel on the operation of the considered system. Typical settings and data used when installing pipelines were chosen. Table 9.8 shows the parameters of regular excitation of the vessel's motion according to (9.98), taking into account the mentioned characteristics of the vessel. All calculations were performed assuming a constant step of integration in the Runge-Kutta method Δh=0.001 s. The notational system used in the subsequent graphs is explained on the scheme presented in Fig. 9.44.

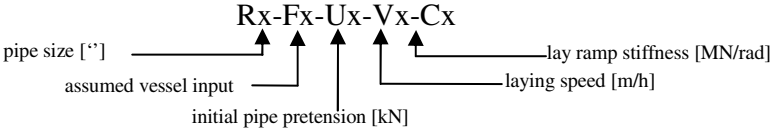

Fig. 9.44. Notations in the results presented on graphs

In Fig. 9.45, the results of calculations for a pipeline with diameter of 4 inches are shown. Graphs of tension indicate significant instability of operation caused by waves and lack of possibility to eliminate undesirably large overloads by changing the braking force of the reel (Fig. 9.45b and c). Fairly stable operation is guaranteed only for modest values of the amplitude of the swaying angle ψ_D when the braking force of the reel is increased (Fig. 9.45a and d). The decay of tension (values of the force U_E near zero in Fig. 9.45b and c) is due to excessive unwinding of the pipe from the reel caused by the increase in the reel's angular velocity (Fig. 9.46).

The graphs of the reel's velocity are shown in Fig. 9.46. The results obtained for F1 and F4 waves (little swaying, Fig. 9.46a and Fig. 9.46d) indicate fairly stable operation of the device in the range of swaying amplitudes from 0 to 1°. Lack of control of the reel's velocity under more intense waves leads to unwinding of great amounts of the pipeline and subsequently to abrupt arrest of the reel (jerk). Increasing the braking force makes it possible to reduce the maximum speed of the reel but it also causes high values of the axial forces which are dangerous to the personnel and the device.

Table 9.7. Main parameters of the device and sizes of pipelines used

Parameter	Value
Admissible mass of the reel together with the wound pipe	$2500 \cdot 10^3$ kg
Range of diameters of steel pipes installed	4"–18"
Designed value of pipes' tension	2500 kN
Capacity of the reel: (for max/min. diameter of the pipeline)	150 km / 7 km
Max/min. Winding diameter of pipes	$D_O = 25$ m / $D_I = 15$ m
Moment of inertia of the reel with the wound pipeline	$2.5 \div 3.0 \cdot 10^8$ kgm^2
Length of the vessel	~100 m
Diameter of the gear wheel	$D_p = 25.7$ m
Link mass m_u of the pipeline for pipe diameter D	$D = 4"$, $m_u = 16$ kg $D = 8"$, $m_u = 42$ kg $D = 12"$, $m_u = 128$ kg $D = 16"$, $m_u = 240$ kg $D = 18"$, $m_u = 340$ kg
Length of the guiding ramp	$L_R = 20$ m
Radius of the ramp's guiding wheel	$r_h = 8$ m
Mass of the ramp with devices	$120 \cdot 10^3$ kg
Distance between the reel and the joint attaching the ramp	$L_H = 55$ m
Ramp inclination angle	$\alpha_R = 60^0$

Table 9.8. Assumed parameters of the vessel's lifting motion

Description	A_X / γ_X, [m]/[°]	A_Y / γ_Y, [m]/[°]	A_ψ / γ_ψ, [m]/[°]	Period of the wave T [s]	Height of the wave H_s [m]	Direction of the wave β_f [°]
F1	0.12/90	0.4 / 75	0.15 / -45	6	3.0	30
F2	0/0	0.45 / 90	2.55 / 20	7	3.0	0
F3	1.0/-100	2.2 / 0	4.1 / 60	8	5.0	60
F4	0.27/-95	0.27 / 0	0.85 / 70	10	1.0	0

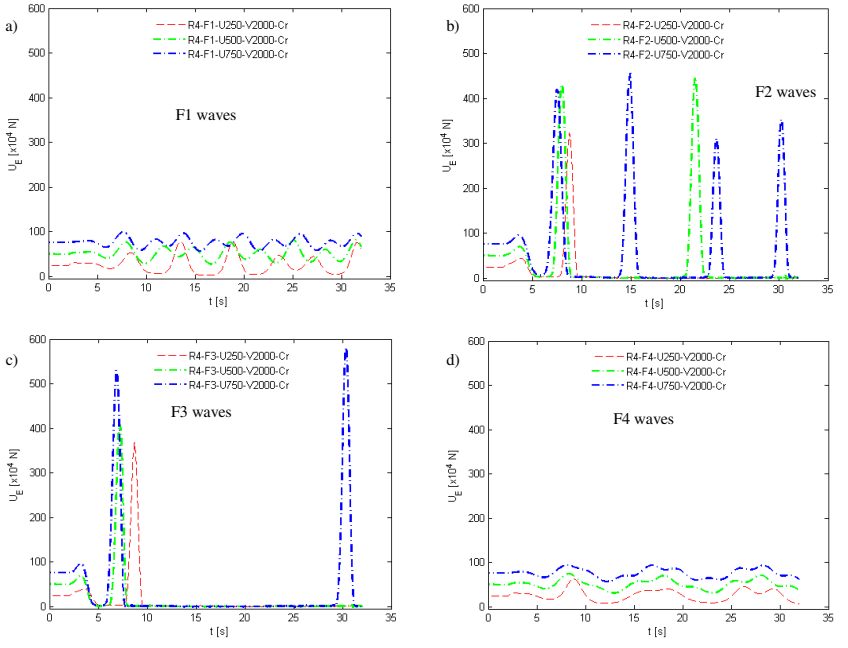

Fig. 9.45. Graphs of tension in the pipeline as it is unwound under waves and with different values of the barking force of the reel: a) ÷ d) correspond to F1 ÷ F4

Multiple factors influence the values of dynamic forces during the device's operation. Among those considered are: flexibility of the guiding ramp's suspension, speed of laying the pipeline, different diameters and load degrees of the reel, value of tension. The results are presented, among other things, in the papers [Szczotka M., 2010], [Szczotka M., 2011a]. In many cases it is impossible to eliminate or significantly reduce dangerously large dynamic forces under wave action with waves of height $H_s > 1$m without using an auxiliary control system. One is proposed in section 10.4.

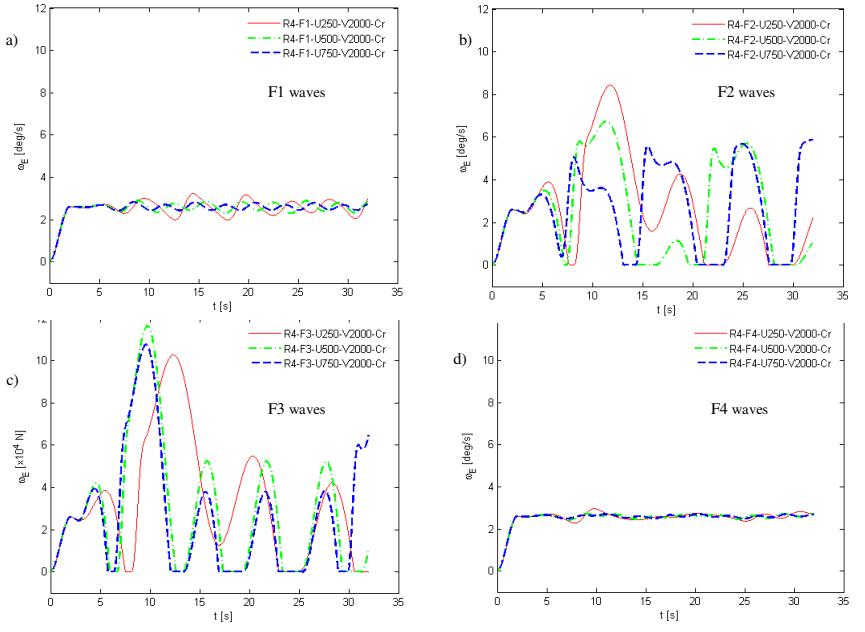

Fig. 9.46. Angular velocity of the reel for different waves conditions and values of braking forces of the reel: a) ÷ d) correspond to F1 ÷ F4